

Graph Convolutional Networks in Multi-modality Medical Imaging: Concepts, Architectures, and Clinical Applications

Authors: Kexin Ding¹, Mu Zhou², Zichen Wang^{3,4}, Qiao Liu⁵, Corey W. Arnold^{3,4}, Shaoting Zhang⁶, Dimitri N. Metaxas⁷

¹Department of Computer Science, The University of North Carolina at Charlotte, Charlotte, USA

²Sensebrain Research, San Jose, USA

³Computational Diagnostics Lab, UCLA, Los Angeles, USA

⁴Department of Bioengineering, UCLA, Los Angeles, USA

⁵Department of Statistics, Stanford University, Stanford, USA

⁶Shanghai Artificial Intelligence Laboratory, Shanghai, China

⁷Department of Computer Science, Rutgers University, New Jersey, USA

**Corresponding to Shaoting Zhang (zhangshaoting@pjlab.org.cn) and Dimitris N. Metaxas (dnm@cs.rutgers.edu)*

Abstract

Image-based characterization and disease understanding involve integrative analysis of morphological, spatial, and topological information across biological scales. The recent surge of graph convolutional networks (GCNs) provides opportunities to address this information complexity via graph-driven architectures. GCNs have demonstrated their capability to perform feature aggregation, interaction, and reasoning with remarkable flexibility and efficiency. These advances of GCNs have prompted a new wave of research and application in medical imaging analysis with an overarching goal of improving quantitative disease understanding, monitoring, and diagnosis. Yet daunting challenges remain for designing the important image-to-graph transformation for multi-modality medical imaging and gaining insights into model interpretation and enhanced clinical decision support. In this review, we share rapid developments of GCNs in the context of medical image analysis including radiology, histopathology, and other related imaging modalities. We discuss the fast-growing synergy of graph network architectures and medical imaging components to advance our assessment of disease status and outcome in clinical tasks. To provide a guideline to foster cross-disciplinary research, we present emerging opportunities and identify common challenges in image-based GCNs and their extensions in model interpretations, technical advancements, large-scale benchmarks to transform the scope of medical image studies and related graph-driven medical research.

1. Introduction

Graph representation has been broadly studied in information extraction, relational representation, and multi-modality data fusion^{1, 2, 3}. The rich topological and spatial characteristics of graphs essentially uncover differential relations among individual graph elements⁴. In medical image analysis, the diverse shape, anatomy, and appearance information provide a key data source to characterize the interactions among the diagnostic region of interests (ROIs) and reveal disease status⁵. Therefore, image-based graph modeling and inference can deepen our understanding of the complex relational patterns hidden in disease tissue regions. The surge of graph convolutional networks (GCNs), a branch of deep learning characterized by graph-level model development, has brought a new wave of information fusion techniques through their widespread applications in medical imaging, from disease classification⁶, tumor segmentation⁷, to patient outcome prediction⁸.

Graph convolutional networks (GCNs) explore the heterogeneous graph data via a series of graph-level convolution, sampling, and enabling the model inference on both graph node attributes and relational structures⁴. The development of GCNs extends conventional graph embedding methods (e.g., Deepwalk⁹ and node2vec¹⁰) primarily on generating a low-dimensional graph representation without considering node attributes. To enable a synergistic analysis with medical imaging, GCNs demonstrate their multifaceted advances on feature extraction, data fusion, and interpretation ability. First, GCNs extract multi-scale spatial relations by characterizing inter- and intra-interactions between different tissue regions, which are vital to understanding disease developmental mechanisms¹. Further, GCNs present a strong fusion capability to handle heterogeneous cross-modality data of both imaging and non-imaging data. The cross-modality analysis is of substantial interest since it can broaden our understanding of disease mechanisms beyond the scope of single modality data. For instance, the brain networks naturally present the relationship between neurons, and the fusion with clinical records can provide auxiliary benefits for brain disease analysis¹¹. Similarly, an integrative analysis of multi-omics profiles and imaging patterns promises to discover novel image-to-genome associations for cancer biomarker discovery^{12, 13}. Finally, GCNs provide a possibility of outcome interpretation by capturing the structural dynamics of complex graphs. The model outcomes can visualize both node distribution and subgraph connectivity derived from the entire graph representation. Taken together, GCNs demonstrate the potential to analyze the abundant amount of graph-level information that is crucial to advance medical imaging understanding and inform decision making in clinics.

A general pipeline for utilizing GCNs in medical imaging is shown in Fig. 1, highlighting key components of multi-modality imaging and clinical data, graph representation frameworks, and downstream clinical applications. To provide a guideline to foster cross-disciplinary research in the field of GCNs and medical imaging, the major contributions of this survey can be summarized as follows:

1. We outline current state-of-the-art GCNs that are widely used in medical image analysis. We summarize the key understanding of their concepts, architectures, and trade-offs of the network architecture design to advance graph and medical imaging research.
2. We highlight the convergence of graph-driven studies in radiological imaging, histopathological imaging, and other imaging modalities. We organize them in a unified taxonomy from the graph construction approaches and their downstream clinical tasks.
3. We offer insights into the image-to-graph transformation that is vital to determine the success of GCNs, including the definition of graph components and different graph construction metrics. This review provides a key reference for researchers to explore the fast-growing synergy between graph architecture and medical imaging components.
4. Emerging opportunities and future directions are discussed in image-based GCNs and their extensions across multiple disciplines. These insights can greatly expand the scope of advancing GCNs in medical imaging and related data-driven medical studies.

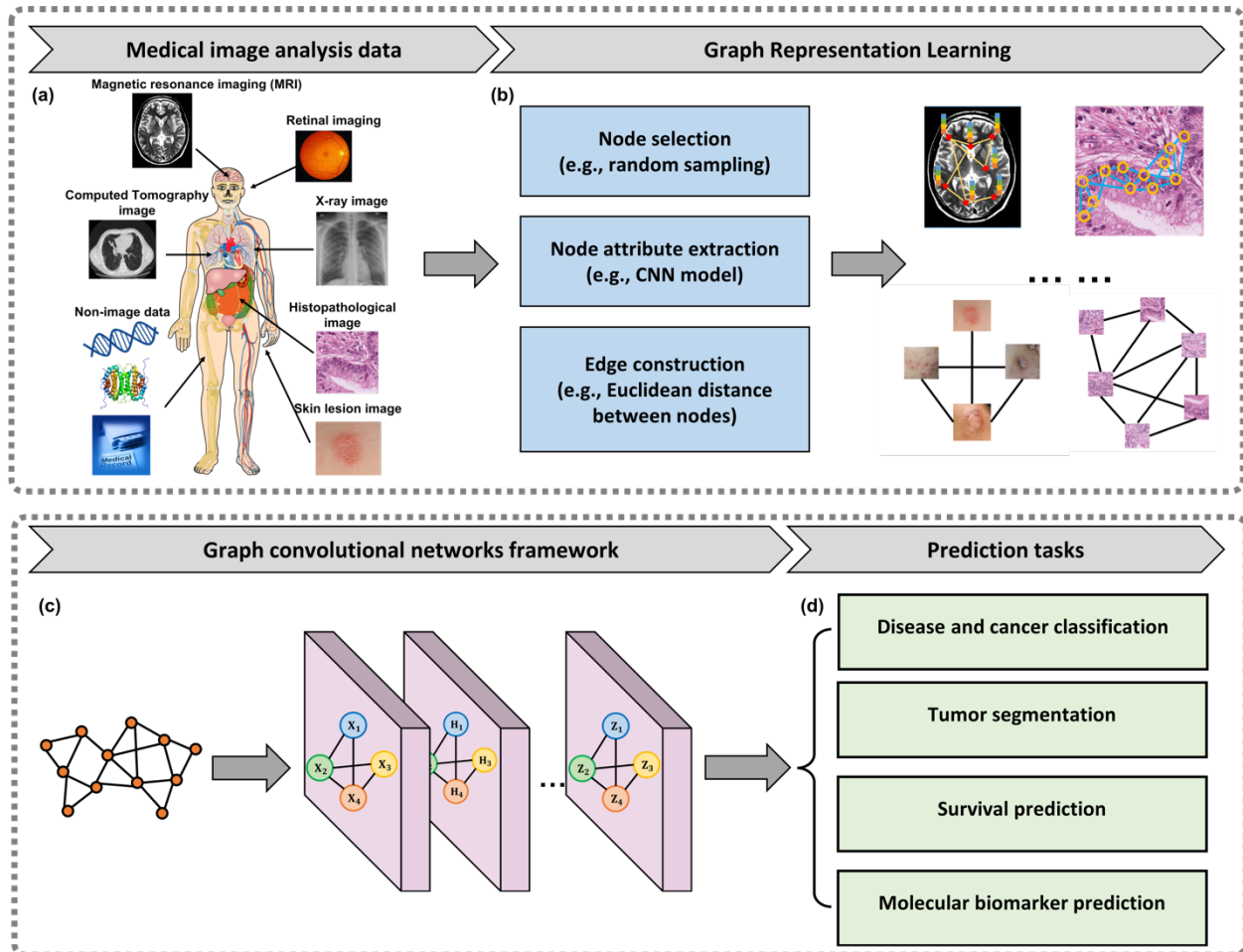


Fig. 1. A general pipeline for utilizing GCNs in medical image analysis. (a) Medical image analysis data. Multi-modality medical imaging and other non-image data can be jointly considered for GCN modeling and

analysis. **(b) Graph representation learning.** The image-graph transformation pipeline includes node selection, node attribute extraction, and edge construction. For different types of medical images, we aim to design a variety of task-specific transformation strategies. **(c) Graph convolutional networks framework.** The input of GCNs is the constructed data-rich graphs based on image contents. The GCNs architecture contains input, hidden, and output layers to allow information extraction and inference. **(d) Clinical tasks.** We review a broad range of tasks with clinical relevance that incorporate disease detection, segmentation, and outcome prediction.

2. Methodology of graph convolutional networks

The architecture of graph convolutional networks (GCNs) essentially addresses the cyclic mutual dependencies with weight parameters in each network layer³. The graph convolutional layer updates graph representations by aggregating node information from their neighborhoods. Also, the edge weights and connections will be updated in specified GCNs applications. Conceptually, GCNs could broadly fall into two categories including spectral-based and spatial-based GCNs. First, the spectral-based graph convolutions are defined in the spectral domain based on the graph Fourier transformation³, which can be regarded as an analogy of the signal Fourier transform in 1-D space. Second, the spatial-based graph convolutions are defined in the spatial domain that the aggregations of node representations come from the collective information of neighboring nodes. Also, we discuss important graph pooling modules as downsampling strategies to reduce the size of graph representation¹, which can critically alleviate issues of overfitting, permutation invariance, and computational complexity in the development of graph neural networks. In later sections, we define a graph as $G = (V, E)$, where V is the graph node and E is the edge between nodes. For graph representation learning, we use H to denote the hidden state vector of nodes.

2.1. Spectral graph convolutional networks

Spectral-based graph convolutional networks are derived from the field of graph signal processing, where the spectral-based convolutional operators are defined in the spectral domain¹. Theoretically, a graph signal x will be transformed to the spectral domain by a graph Fourier transform \mathcal{F} before the convolution operation. In this way, the spectral-based graph convolutions can be computed by taking the inverse Fourier transform of the multiplication between two Fourier transformed graph signals⁵. Then the resulting signal is transformed back by the inverse graph Fourier transform \mathcal{F}^{-1} . These transformations are defined as:

$$\mathcal{F}(x) = U^T x, \quad (1)$$

$$\mathcal{F}^{-1}(x) = Ux, \quad (2)$$

U is the matrix of eigenvectors of the normalized graph Laplacian matrix $L = I_N - D^{-\frac{1}{2}}AD^{-\frac{1}{2}}$, where I_N is the normalized identity matrix, D is a node degree matrix and A is the adjacency matrix, which represents the connectivity between every two nodes. L has the property of being real symmetric positive semidefinite. With this property, the normalized Laplacian matrix can be factorized as $L = U\Lambda U^T$, where Λ is a diagonal matrix of all the eigenvalues. According to the graph fourier transformation, the input graph signal x with a filter $g \in R^n$ is defined as:

$$g \star x = \mathcal{F}^{-1}(\mathcal{F}(g) \odot \mathcal{F}(x)) = U(U^T g \odot U^T x), \quad (3)$$

where \odot denotes the element-wise product, $U^T g$ is a filter in the spectral domain. If we simplify the filter by a learnable diagonal matrix $g_\theta = \text{diag}(U^T g)$, then the spectral graph convolution can be simplified as:

$$g_\theta \star x = U g_\theta U^T x, \quad (4)$$

The majority of spectral-based graph convolutional networks are based on the above definitions, and the design of filter g_θ determines the various performance of individual approaches. Normally, the spectral-based graph convolutional network designs the convolution operation in the Fourier domain by computing the eigen-decomposition of the graph Laplacian². They assume that the filter $g_\theta = \theta_{i,j}^{(k)}$ is a set of learnable parameters and considers graph signals with multiple channels. Due to the eigen-decomposition of the Laplacian matrix, any perturbation to a graph can result in changes of eigenbasis³. The learned filters are domain dependent with a poor graph structure generalization. Also, eigen-decomposition has a high computational complexity that is unfavorable for large-scale data processing. To overcome the limitations, especially the computational complexity, Chebyshev spectral CNN (ChebNet)¹⁴ used K-polynomial filters to achieve a good localization in the vertex domain by integrating the node features within the K-hop neighborhood, i.e. $g_\theta = \sum_{i=0}^k \theta_i T_i \bar{L}$ (4), where $\bar{L} = \frac{2}{\lambda_{max}} L - I_N$, λ_{max} denotes the largest eigenvalue of L. The range of the eigenvalues in \bar{L} is [-1,1]. The Chebyshev polynomials are defined recursively as $T_i(x) = 2x T_{i-1}(x) - T_{i-2}(x)$ with $T_0(x) = 1$ and $T_1(x) = x$. The convolution operation can be written as:

$$g_\theta \star x = \sum_{i=0}^k \theta_i T_i \bar{L} x, \quad (5)$$

For a similar purpose of improving computational efficiency, CayleyNet¹⁵ applies the Cayley polynomials that are parametric rational functions to capture narrow frequency bands. The spectral graph convolution operation is defined as:

$$g_\theta * x = c_0 x + 2\operatorname{Re}\left\{\sum_{j=1}^r c_j (hL - iI)^{-j} x\right\}, \quad (6)$$

Where $\operatorname{Re}(\cdot)$ returns the real part of a complex number, c_0 is a real coefficient, c_j is a complex coefficient, i is the imaginary number, and h is the parameter that controls the spectrum of a Cayley filter. ChebNet could be regarded as a special case of CayleyNet via the use of the Chebyshev polynomial approximation to reduce the computational complexity.

A notable variant of ChebNet for further simplifying the computational complexity, which truncates the Chebyshev polynomial to the first-order approximation that the central node only considers its 1-hop neighboring nodes¹⁶. The approach simply filters in (5) with $i=1$ and $\lambda_{max} = 2$ to alleviate the problem of overfitting:

$$g_\theta * x = \sum_{i=0}^k \theta_i T_i \bar{L} x \approx \theta_0 x + \theta_1 (L - I_N) x = \theta_0 x - \theta_1 D^{-\frac{1}{2}} A D^{-\frac{1}{2}} x, \quad (7)$$

To restrain the number of parameters and avoid overfitting, GCN further assumes that $\theta = \theta_0 = \theta_1$ so that $g_\theta = \theta(I_N + D^{-\frac{1}{2}} A D^{-\frac{1}{2}})$. To solve the exploding or vanishing gradient problem in (7): $I_N + D^{-\frac{1}{2}} A D^{-\frac{1}{2}} \rightarrow \bar{D}^{-\frac{1}{2}} \bar{A} \bar{D}^{-\frac{1}{2}}$, with $\bar{A} = A + I_N$ and $\bar{D}_{ij} = \sum_j A_{ij}$. The propagation layer of GCN is defined as:

$$H = \bar{D}^{-\frac{1}{2}} \bar{A} \bar{D}^{-\frac{1}{2}} X \theta, \quad (8)$$

where $X \in R^{N \times F}$ is the input matrix, $\theta \in R^{N \times F'}$ is the parameter and $H \in R^{N \times F'}$ is the output matrix. F and F' are the dimensions of the input and the output, respectively.

Recent research findings demonstrate the improvement of GCN's feasibility and consistency on graph models. The adaptive graph convolution network (AGCN)¹⁷ could construct and learn a residual graph Laplacian matrix for each sample in the batch through a learnable distance function that takes two nodes' features as inputs. The residual graph Laplacian matrix leads to achieving high-level performance in public graph-structured datasets. In addition, the dual graph convolutional network (DGCN)¹⁸ explores the perspective of augmenting the graph Laplacian as AGCN¹⁷. DGCN jointly considers the local consistency and global consistency on graphs through two convolutional networks. The first convolutional network is the same as (8), while the second network replaces the adjacency matrix with the positive pointwise mutual information (PPMI) matrix.

Spectral-based graph convolutional networks have a solid theoretical foundation derived from graph signals theories. Despite efforts to overcome the computation complexity, the generalization power of spectral-based

GCNs is limited as opposed to the broad usage of spatial-based approaches below. Currently, the spectral-based methods train the filters on the fixed graph structure, making the trained filters unable to apply to a new graph with different structures. However, the graph structures can dramatically vary in both size and connectivity in practical applications¹⁷. The generalization power across different tasks and the high computation complexity become the major hurdles to developing spectral-based graph convolutional networks.

2.2. Spatial graph convolutional networks

The spatial graph convolutional operation essentially focuses on aggregating and updating node representation by propagating node information along edges³. The aggregation strategy can directly improve the generalization power of dealing with different structured graphs by aggregating the information from neighboring nodes and updating the center node representation.

The message-passing neural network (MPNN)¹⁹ represents a general framework of spatial-based GCNs³. The key forward propagation strategy of MPNN is passing the information between nodes through edges directly. As defined in the propagation function below, MPNN runs T steps message-passing iterations so that the information could be propagated between nodes. Notably, GraphSAGE²⁰ is a general inductive framework which generates embeddings by sampling and aggregating features from a node's local neighborhood. GraphSAGE leverages node feature information to efficiently generate node embeddings for previously unseen data²⁰.

The propagation rule follows:

$$h_{N(v)}^k = \text{AGGREGATE}_k(\{h_u^{k-1}, \forall u \in N(v)\}), \quad (10)$$

$$h_v^k = \sigma(W^k \cdot \text{CONCAT}(h_v^{k-1}, h_{N(v)}^k)), \quad (11)$$

Where AGGREGATE is an aggregator function that could aggregate information from node neighbors. Three types of aggregators are utilized in GraphSAGE, including mean aggregator, LSTM aggregator, and pooling aggregator. W^k is a set of weight matrices that are used to propagate information from different layers. CONCAT is the concatenated operation. Interestingly, GraphSAGE with a mean aggregator can be considered as an inductive version of GCN. To further identify the graph structures that cannot be distinguished by GraphSAGE²⁰, Graph Isomorphism Network (GIN)²¹ is a maximally powerful architecture to distinguish the isomorphism graph. As proved in GIN²¹, the injective aggregation update maps node neighborhoods to different feature vectors so that the isomorphism graph can be distinguished. To achieve the injectivity of the AGGREGATE, sum-pooling is applied in GIN. The AGGREGATE and COMBINE steps are integrated as follows:

$$h_v^{(k)} = \text{MLP}^{(k)}((1 + \epsilon^{(k)}) \cdot h_v^{(k-1)} + \sum_{u \in N(v)} h_u^{(k-1)}), \quad (12)$$

MLP is a multi-layer perceptron that could represent the composition of functions.

The attention mechanism has been increasingly applied in spatial-based GCNs models for various sequence-based approaches^{1,22}. Several key works are attempting to utilize attention mechanisms on graphs. Different from the design of spectral and spatial convolutional operations, the attention-based convolutional operations assign different weights for neighbors to stabilize the learning process and thus alleviate noise effects. A benefit of attention mechanisms is that they allow for dealing with variable-sized inputs, and focusing on the most relevant parts of the input to make decisions²². Graph Attention Network (GAT)²² proposes a computationally efficient graph attentional layer which leverages self-attention and multi-head attention mechanisms. The GAT layer is parallelizable across all nodes in the entire graph while allowing for assigning different importance weights to different (degree) nodes in different size neighborhoods, and does not depend on knowing the entire graph structure. The coefficients computed by the attention mechanism and the propagation of GAT is formulated as:

$$\alpha_{ij} = \frac{\exp(\text{LeakyReLU}(\alpha^T [Wh_i || Wh_j]))}{\sum_{k \in N_i} \exp(\text{LeakyReLU}(\alpha^T [Wh_i || Wh_k]))}, \quad (13)$$

$$h'_i = \sigma(\sum_{k \in N_i} \alpha_{ij} Wh_j), \quad (14)$$

where α and W are weight vectors, and $||$ is the concatenation operation.

Furthermore, GAT leverages multi-head attention²³ to stabilize the learning process of self-attention (14), which can be written as,:

$$h'_i = \prod_{k=1}^K (\sum_{j \in N_i} \alpha_{ij}^k Wh_j), \quad (15)$$

$$h'_i = \sigma(\frac{1}{K} \sum_{k=1}^K \sum_{j \in N_i} \alpha_{ij}^k W^k h_j), \quad (16)$$

where α_{ij}^k are normalized attention coefficients computed by the k -th attention mechanism. GAT achieved significant improvement in both transductive tasks and inductive tasks, especially in the inductive task (e.g., protein-protein interaction dataset), GAT improved the micro-averaged F1 scores by 20.5% compared to the best GraphSAGE result.

In summary, spatial-based convolutional graph operations follow a neighborhood aggregation strategy, where we can iteratively update the representation of a node by aggregating representations of its neighbors. After k iterations of aggregation, a node's representation captures the structural information within its k -hop network neighborhood. The rapid development of spatial-based GCNs has displayed their computational efficiency, graph-structure flexibility, and potential generalization across tasks while compared with spectral-based GCNs³. First, spatial-based GCNs tend to be more efficient than spectral-based GCNs because they directly

perform convolutions in the graph domain via node information propagation. Thus spatial-based GCNs do not have to perform eigenvector computation or handle the whole graph computation simultaneously. Second, spatial-based models are flexible to handle multi-sourced graph inputs via the convenient aggregation function³. These graph inputs can be prepared as edge inputs^{24, 25, 26, 27, 28}, directed graphs^{29, 30}, signed graphs³¹, and heterogeneous graphs^{32, 33}. Third, spatial-based models perform graph convolutions locally on each node where network weights can be efficiently generalized across different nodes and graph structures. Therefore, spatial-based models have been shown to achieve superior performance on both transductive (e.g., semi-supervised learning) and inductive (e.g., the traditional supervised learning) tasks with flexibility on graph structures.

2.3. Graph pooling mechanisms

Graph pooling is a key strategy to address the computational challenges derived from graph convolutional operations³⁴. Pooling operations reduce the size of a graph representation while preserving valuable structural information. Typically, graph pooling layers are located after graph convolutional layers and work as a down-sampling strategy. Graph pooling can be categorized into global and hierarchical graph poolings as shown in Fig. 2.

Global pooling operation aggregates the node representations via simple flattening procedures such as summing, averaging, or maxing the node embeddings that are widely used in graph classification tasks³⁴. Further, a global sorting pooling³⁵ sorts the node features in a descending order based on their last feature channel and the k -largest nodes form the updated graph representation of the global sorting pooling layer. Also, global attention pooling³⁶ acts as a soft attention mechanism that decides relevant nodes to the current graph-level task. Such global-wise pooling strategies, also known as readout layers, are often used to generate graph-level representation based on the previous node representations.

Hierarchical pooling operation is designed to refine the node representation by down-sampling strategies and overcome model overfitting. Hierarchical pooling strategies could be further categorized into two types including clustering-based and sorting-based methods. In clustering methods, spectral clustering (SC) offers an efficient means to find strongly-connected communities on a graph. SC can be used in GCNs to implement pooling operations that aggregate nodes especially belonging to the same cluster³⁷. However, the expense of eigen-decomposition of the Laplacian and the generalization of SC strategies remain yet to be explicitly addressed. Alternatively, a graph clustering approach³⁷ formulates a continuous relaxation of the normalized min-cut problem and trains GCNs to compute cluster assignments. Spatial-based clustering strategies are proposed to achieve a higher computation efficiency compared with spectral-based clustering strategies. For

example, DIFFPooling³⁸ is a differentiable graph pooling strategy that can generate hierarchical representations of graphs and can be combined with various GCNs architectures in an end-to-end fashion³⁸. The key design of DIFFPooling is to learn a differentiable soft cluster assignment for nodes at each GCNs layer and mapping nodes to a set of clusters, which then forms the coarsened input for the next GCNs layer. In sorting-based methods, they focus on updating the node representation by sorting the nodes and edges depending on their attributes or weights. TopKPooling and SAGPooling shared a similar idea on the node sorting by their attention scores^{39, 40, 41, 42}. These poolings are designed to help select the top-kth nodes to summarize the entire graph for further feature computations. Notably, TopKPooling and SAGPooling can drop the node during model training to improve the computation efficiency and thus overcome the model overfitting. From the graph edge perspective, EdgePooling^{43, 44} is an inspiring example that could drop edges and merge nodes by sorting all edge scores and successively choosing the useful edges with the highest score whose two nodes have not yet been part of a contracted edge.

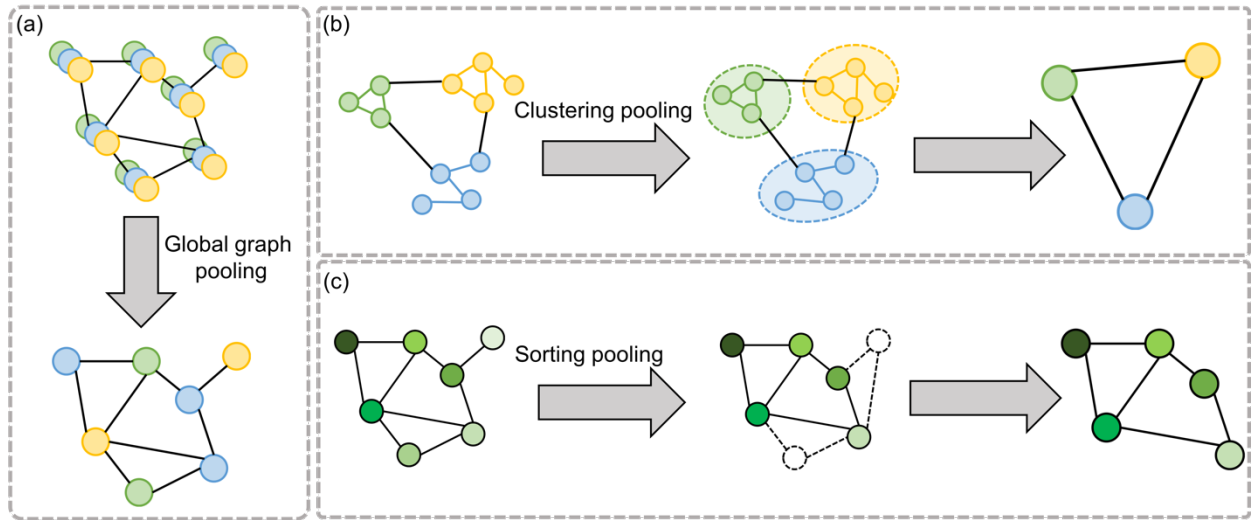


Fig. 2. Graph pooling mechanism. **(a) Global graph pooling.** The function of global graph pooling is to flatten the node representations to a graph representation. In node representation, each node will include multiple dimensions of node attributes. After utilizing the global graph pooling, the most representative feature will be selected as the node attribute in graph representation. **(b) Clustering graph pooling.** Clustering-based poolings offer an efficient means to find strongly-connected communities on a graph. The nodes in the same clusters are represented by a new cluster node representation. **(c) Sorting graph pooling.** Sorting-based pooling updates the node representation by sorting the nodes attributes or edges weights. Both (b) and (c) are hierarchical pooling operations that refine the node representation to gain model robustness and improve computation efficiency.

2.4. Trade-offs in the design of GCNs architectures

To optimize the performance of graph network models, there are multiple trade-offs between the network architecture and the corresponding model performance. The ability of information collection and the strategy of effective aggregation are crucial factors for measuring the performance of GCNs models. Intuitively, a deeper architecture corresponds to a larger receptive field, which can collect more auxiliary information towards enhanced performance of GCNs. However, the performance might decrease when layers go deeper to evolve larger receptive fields in real applications²⁵. Such performance deterioration could be attributed to the over-smoothing of node representation with an increased architecture depth. In other words, the repeated and mixed message aggregation can lead to node representations of inter-classes indistinguishable⁴⁵. It is commonly seen that the over-smoothing issue always occurs in the nodes with a dense connection with other nodes (e.g., the core of the graph) that could rapidly aggregate information in the entire graph. In contrast, the node in the tree part (e.g., leaves of the tree) could only include a very small fraction of information of all nodes with a small number of GCNs layers. To improve the GCNs model performance, it is necessary to overcome the graph over-smoothing phenomena and achieve informative node representation. For example, the study⁴⁶ implemented a co-training and self-training scheme with a smoothness regularizer term and adaptive edge optimization⁴⁵ to alleviate the over-smoothing problem. Co-training a GCN with the random walk model can explore the global graph topology. Further, self-training a GCN could exploit feature extraction capability to overcome its localized limitation. Informative node representation via the jumping knowledge network (JK-Net)⁴⁷ tends to demonstrate compelling performance on graph computing efficiency and alleviate overfitting. Notably, the idea of layer-aggregation across layers helps select the most informative nodes and reduce the overfitting issue, and the LSTM-attention could further identify the useful neighborhood ranges. Inspired by the architecture of JK-Net, Deep adaptive graph neural network (DAGCNs)²⁵ developed an adaptive score calculation scheme for each layer, which could balance the information from both local and global neighborhoods for each node. Both JK-Net and DAGCNs aim to find a trade-off between accuracy performance and the size of receptive fields by adaptively adjusting the information from local and global neighborhoods. For the design of network architecture, we expect additional efforts to overcome the over-fitting issues while keeping a flexible architecture to explore more meaningful information in the context of disease detection and diagnosis.

3. Development of GCNs in medical imaging

3.1 Radiological image analysis

Over the past decades, multi-modality radiological images have been routinely utilized in abnormality segmentation^{48, 49}, detection^{50, 51}, and patient outcome classification^{52, 53}. In this section, we discuss the growing body of GCNs studies applied to radiological analysis^{54, 55, 56}, including magnetic resonance imaging (MRI), Computed Tomography (CT), and X-ray imaging. The combination of GCNs and radiological imaging promises

to reflect the interaction among tissue regions and provide an intuitive means to fuse the morphological and topological-structured features among key image regions to advance modeling, interpretation, and outcome prediction. We here discuss the representative neuroimaging research and other related studies to highlight the usefulness of GCNs across different radiological imaging modalities and clinical tasks.

3.1.1 Neuroimaging

In neuroimaging, multi-modality MRI is a useful diagnostic technique by providing high-quality three-dimensional (3D) images of brain structures with detailed structural information⁵⁷. Conceptually, multi-modality MRI data can be categorized into functional MRI (fMRI), structural MRI (sMRI), and diffusion MRI (DMRI). The fMRI measures brain activity and detects the changes in blood oxygenation and blood flow in response to neural activity⁵⁸. The sMRI translates the local differences in water content into different shades of gray that serve to outline the shapes and sizes of the brain's various subregions⁵⁹. The DMRI is a magnetic resonance imaging technique in which the contrast mechanism is determined by the microscopic mobility of water molecules⁶⁰. All these imaging modalities provide vital diagnostic support for neurological disease analysis because they can capture anatomical, structural, and diagnosis-informative features in neurology. Therefore, the overarching goal is to develop useful graph network models to define, explore, and interpret interactions of brain neurons and tissues. The detailed process of utilizing GCNs in the neuro-imaging analysis is illustrated in Fig. 3.

To analyze the complex brain region connectivity and interaction, a brain graph representation can intuitively portray human brain organization, neurological disorders, and associated clinical diagnosis. Conventionally, the human brain could be modeled into a brain biological network containing nodes (e.g., region of interests) and edges among brain network nodes. The edges could be determined by brain signals or the real fiber connection. Yet these biologically-defined networks are often unable to faithfully capture neurological disorders and outcomes of patients⁶¹. To overcome this challenge, it is encouraged to leverage informative image-based features to considerably enrich graph node attributes. Comprehensive graph representation can integrate multiple types of information (e.g., image features, human brain signals, and clinical data) to greatly expand the knowledge base of brain dynamics and potentially provide auxiliary clinical diagnosis assistance. The use of GCNs here can be helpful to augment the architecture of human brain networks and has achieved remarkable progress in explaining the functional abnormality from the network mechanism⁶². In particular, GCNs are able to consider the functional or structural relations among brain regions together with image-based features that are beyond the scope of the conventional CNN-based methods^{63, 64, 65}. The CNN-based model is merely viewed as a feature extractor for disease representation without consideration of structure information of the brain. For example, the deep 3-D convolutional neural network architecture was not unable to capture underlying structure information for Alzheimer's disease classification using brain MRI scans⁶¹. By contrast,

the convergence of GCNs methods and MRI provide an alternative means to characterize the architecture of human brain networks and has achieved outstanding progress in brain abnormality explanation⁶².

The graph representations can be divided into functional and structural brain connectivity graphs based on the definitions of the graph components. First, graph nodes are regions of interest (ROI) as defined in MRI. ROI definition is commonly done through the anatomical parcellation of the Montreal neurological institute (MNI) using sMRI and fMRI data^{66, 67, 68}. Second, graph edges are determined by the physical connectivity (e.g., the fiber tracts) of nodes in structural brain networks while calculated from the signal series analysis in functional brain networks. We therefore discuss insights of functional and structural brain connectivity graph developments below.

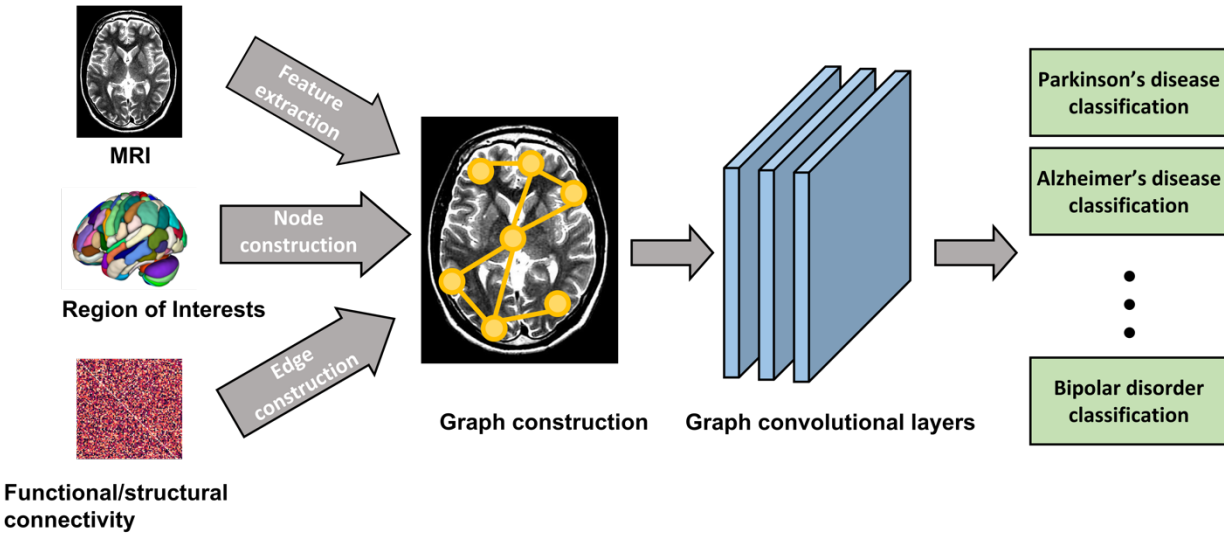


Fig. 3 The framework of developing GCNs in neuro-imaging analysis. Multi-modality MRIs are firstly converted into graph structure which is determined by the region of interest in terms of real human brain signals or fiber connectivity (e.g., node and edge definitions). Through graph-level model development and inference, we highlight numerous image-based analysis and diagnosis of diseases in neurology.

The human brain functional connectivity denotes the functional relations between specific human brain areas and functional brain graphs can represent estimates of interactions among time series of neuronal activity⁶². In functional brain networks, the nodes are defined as brain parcellation ROIs while the node attributes could be hand-crafted features or correlation measurements between nodes. The edges are created through the node correlations between different regions. For example, the GCNs framework achieved high-level performance in classifying Autism spectrum disorders (ASD) and healthy controls (HC) using task-functional magnetic resonance imaging (task-fMRI) through the appropriate ROI definition⁶⁹. Their model consists of a message-passing neural network (MPNN)¹⁹ as convolutional layers that is invariant to graph symmetries⁶⁹. Furthermore, Top-k poolings³⁹ is able to downsample the node to achieve a higher computation efficiency while preserving

a meaningful graph delineation. For a similar ASD and HC classification, another study⁷⁰ used GAT²² as the convolutional layer incorporated with Top-k^{39, 40} and SAGE⁴² pooling for achieving node importance scores. They also introduced two distance losses to enhance the distinguish among the nodes. Also, a group-level consistency loss is added to force the node importance scores to be similar for different input instances in the first pooling layer. Inspired by metric learning, a siamese graph convolutional neural network (s-GCN) is proposed for the ASD and HC classification purpose⁵⁴, where samples were collected from Autism Brain Imaging Data Exchange (ABIDE)⁷¹ database and UK Biobank⁷². The graph metric learning method essentially utilized GCN layer¹⁶ in a siamese network⁷³. Two types of graph construction methods are designed as the input of the model, such as spatial and functional graphs which determine nodes by ROIs, meanwhile, the KNN algorithm is utilized for both spatial and functional graph construction. The inputs for s-GCN are two same structure spatial or functional graphs with different signals (e.g., rows or columns of functional matrix). Notably, the spatio-temporal graph could be used to analyze the functional dependency between different brain regions and the information in the temporal dynamics of brain activity simultaneously. The spatio-temporal graph convolutional network is utilized to analyze the Blood-oxygen-Level-dependent (BOLD) signal of resting-state fMRI (rs-fMRI) for human age and sex prediction⁷⁴. Also, studies^{75, 76} analyze the BOLD signal of fMRI for accurate detection of cognitive state changes of the human brain by presenting a dynamic graph learning approach to generate an ensemble of subject-specific dynamic graph embeddings. The brain networks are able to disentangle cognitive events more accurately than using the raw BOLD signals. The functional graph is meaningful to reflect the average functional connection strength between pairs of brain regions within a population. Generally, Pearson's correlation is a useful strategy to construct functional connectivity matrix and define the node attributes.

The human brain's structural connectivity *in vivo* can be captured by structural and diffusion MRI^{77, 78}, and structural brain graphs could represent anatomical wiring diagrams⁶². Similar to the definition of nodes in functional connectivity networks, the nodes in structural connectivity networks are defined as a region of interests (ROIs), which are parceled from the brain based on structural and diffusion MRI. Clinically, the structural brain connectivity represents the structural associations of altered neuronal elements, including both the morphometric alternation and accurate anatomical connectivity as seen in imaging. In the complex brain networks, structural brain connectivity assesses to white amount projections bond cortical and subcortical regions⁷⁹. The edges indicate the actual neural fiber connections between different brain regions. For example, a stack architecture design of combining a heterogeneous GCN model⁵⁵ with an efficient adaptive pooling scheme³⁸ is able to predict the clinical score of Parkinson's disease (PD) and HC using diffusion-weighted MRI (DWI) on Parkinson Progression Marker Initiative (PPMI)⁸⁰. To construct the graph structure from DWI, nodes are defined by the ROIs in the brain while three whole-brain probabilistic tractography algorithms are able to determine different brain structural. The node attributes corresponding to rows in the human brain network are defined as features. Another novel framework is developed to explore graph structure in the q-space by representing DMRI data and utilizing graph convolutional neural networks to

estimate tissue microstructure⁸¹. This approach is capable of not only reducing the data acquisition time but also accelerating the estimation procedure of tissue microstructure. The nodes of the weighted graphs are sets of points on a manifold. Also, the adjacency weights are defined between two nodes using Gaussian kernels, accounting for differences in gradient directions and diffusion weightings. The q-space signal measurements are represented by using the constructed graph that encodes the geometric structure of q-space sampling points. A residual ChebNet¹⁴ can learn the mapping between sparsely sampled q-space data and high-quality estimates of microstructure indices.

Beyond single-modality MRI analysis, multi-modality image data analysis emerged as active research areas for GCNs modeling. Multi-modality MRI data analysis is able to deepen our understanding of disease diagnosis from different data aspects. In neuroimaging, the structural connectivity in sMRI reflects the anatomical pathways of white matter tracts connecting different regions, whereas the functional connectivity in fMRI encodes the correlation between the activity of brain regions. A unique advantage of multi-modality MRI data analysis is that they have incorporated complementary information from different modalities simultaneously. The multimodal data fusion can be implemented by two types of strategy: (1) constructing the original graphs directly using the partial information from functional and structural brain connectivity; (2) constructing the original functional and structural graphs separately and updating the graph representations by computing and fusing the two-side information. For the first fusion strategy, the study⁸² introduced an edge-weighted graph attention network (EGAT)²² with a diffPooling³⁸ to classify Bipolar disorder (BP) and HC from sMRI and fMRI in cerebral cortex analysis. Also, the framework of Siamese community-preserving graph convolutional network (SCP-GCN)⁸³ is able to learn the structural and functional joint embedding of brain networks on two public datasets (i.e., Bipolar and HIV dataset⁸³) for brain disease classification. Especially, siamese architecture can exploit pairwise similarity learning of brain networks to guide the learning process to alleviate the data scarcity problem⁸³. Ninety cerebral regions are selected as nodes for both structural (e.g., Diffusion Tensor Image (DTI)) and functional (e.g., fMRI) networks, and the node attribute is determined by the functional connectivity between nodes corresponding to fMRI. The edge connectivity is determined by the DTI via a series of preprocessing (distortion correction, noise filtering, repetitive sampling from the distributions of principal diffusion directions for each voxel). To preserve the community property of brain networks, the design of a community loss presents its usefulness to minimize the intra-community loss and maximize the intercommunity loss. For the second fusion strategy, the study⁸⁴ fused information from multimodal brain networks on rs-fMRI and dMRI for age prediction. After constructing the original functional and structural brain networks separately, the study reconstructed the positive and negative connections in the functional networks depending on structural networks' information. They utilized a multi-stage graph convolutional layer, motivated by GAT²² and ResGCN⁸⁵, for structural network edge feature update and class classification. Then, the edge feature and class are utilized to update the functional networks for age prediction. Also, for liver lesion segmentation, a mutual information-based graph co-attention module^{86,87} is proposed by extracting modality-specific features from T1-weighted images (T1WI) and establishing the regional correspondence from T2-

weighted images (T2WI) simultaneously. In this study, they constructed two separate graphs for either T1WI or T2W2; meanwhile, they used GCN¹⁶ to propagate representations of all nodes. The mutual information-based graph co-attention module updates the T1WI-based node representation by selectively accumulating information from node features from T2WI-based node representation. The fused node representation is re-projected and added to the original feature for the final segmentation.

Furthermore, GCNs extend to allow the multi-modality integration between MRI and non-imaging data for analyzing complex disease patterns. For example, an Edge-Variational GCN (EV-GCN)¹¹ could automatically integrate imaging data (e.g. fMRI data) with non-imaging data (e.g. age, gender and diagnostic words) in populations for uncertainty-aware disease prediction. They constructed weighted graphs via an edge-variational population graph modeling strategy. In the weighted graphs, the graph nodes are ROIs and the node attributes are features extracted from histology and fMRI images. It is particularly notable that the weight of the edge is achieved by a learnable function of their non-imaging measurements. The proposed Monte-Carlo edge dropout randomly drops a fraction of edges in the constructed graphs to reduce overfitting and increase the graph sparsity. In addition, two similar studies^{88, 89} constructed the sparse graph by combining the information from the functional connectivity (e.g., rs-fMRI), structural connectivity (e.g., DTI), and demographic records (e.g., gender and age) for mild cognitive impairment detection and classification. In these studies, they constructed functional and structural brain networks for each subject (e.g., image). Then, they defined each subject as graph node. For the first study⁸⁸, they concatenated the feature from functional and structural connectivity as vertices features. Also, they calculate the feature and phenotypic information similarity to constructed graph edges. Further, they utilized GCN¹⁶ incorporated with the random walk algorithm to enhance the detection performance. For the second study⁸⁹, it constructed graphs for the functional and structural connectivity separately. Beyond the similarity evaluation of subjects (e.g., vertices) feature and non-image phenotypic information, this study also determined the edge by connecting nodes belong to the same receptive field class directly. Further, they used the constructed graph to pretrain GCN to update graphs and GCN for the final disease deterioration prediction.

3.1.2 X-ray and CT imaging

Extensive studies have also utilized GCNs in X-ray and Computed Tomography (CT) images for disease analysis^{56, 90, 91}. Different from MRI data, CT images are able to reflect the vessel skeleton information that could assist a variety of clinical tasks. For example, chest CT scans can assist with arteries-veins separations that are of great clinical relevance for chest abnormality detection⁹⁰. The graph was constructed of the voxels on the skeletons resulting in a vertex set and their connections in an adjacency matrix. The skeletons are extracted from chest CT scans by vessel segmentation and skeletonization. In this study⁹⁰, GCN layers can extract and learn connectivity information. The one-degree (direct) neighbors were considered and the vertices attributes were extracted by CNN model to consider the local image information. In addition, chest CT scans together with

GCN is able to assist airway semantic segmentation, which refers to the segmentation of airway from background and dividing it into anatomical segments for lung lobe analysis⁹². Also, a prototype-based GCN framework⁹³ provided a means for airway anomaly detection to aid in lung disease diagnosis. The GCN layers calculated the initial anomaly score for every node, while the prototype-based detection algorithm computed the entire graph's anomaly score. Another study⁹⁴ utilized radiotherapy CT (RTCT) and PET, which is registered to the RTCT for lymph node gross tumor volume (GTV_{LN}) detection. In this study, the 3D CNN extracted instance-wise visual features while the GNN model analyzed the inter-LN relationship. The feature fusion of CNN and GNN boosted the GTV_{LN} detection performance. Furthermore, the study⁹⁵ utilized GCN¹⁶ on cone-beam computed tomography (CBCT) images for craniomaxillofacial (CMF) landmark localization, which is important for designing treatment plans of reconstructive surgery. They utilized an attention feature extraction network for localizing landmarks and generating attention features for the graph construction. In addition, the study⁵⁶ proposed an end-to-end hybrid network to train a CNN and GAT network to leverage both advanced feature learning and inter-class feature representations on Chest-Xray 14 dataset⁹⁶. To utilize the image sequencing information, they determine each image from the same patient as a vertice of a graph and the extracted features are the attributes of vertices. Furthermore, they leverage non-imaging meta-data, such as clinical information, to construct edges between the vertices. After constructing the graph and updating the graph representation with GAT, they combine the CNN extracted features with graph representation by skip-connectivity to achieve hybrid representation. The motivation of generating hybrid representation is to improve the distinction between samples. Furthermore, CT images and non-image clinical information could be analyzed jointly for Lymph node metastasis (LNM) prediction. The study⁹⁷ proposed a co-graph convolutional layer consisting of Con-GAT²² and Corr-GAT⁹⁸ layers to achieve the node's new representation by weighted averaging its neighboring nodes and measuring the weight score by feature difference-based correlation. Due to the pandemic of COVID-19, GCNs have also been utilized in disease detection. GraphCovidNet⁹¹ utilized GIN for COVID-19 detection on both CT and X-ray images. The graph is used to depict the outline of an object (e.g., organ) in the image. First, they applied edge detection to determine the edge outline. Then, the graph nodes are defined by the pixel having a grayscale intensity value greater than or equal to 128, which implies nodes reside only on the prominent edges of the edge image. The node attribute consists of the grayscale intensity of the corresponding pixel. An edge exists between the two nodes which represent neighboring pixels in the original image. For example, the GCN model⁹⁹ extracts node information hierarchically towards both diagnosis and prognosis for COVID-19 patients. Their distance-aware pooling, including graph-based clustering and feature pooling, is able to aggregate node information on the dense graph effectively. Also, the proposed model could coarsely localize the most informative slices for CT scans to provide the interpretability for better clinical decision-making.

Table1 summarizes a variety of graph construction methods and GCNs application in radiologic image analysis. Compared to conventional methods, GCNs methods for the analysis of brain networks have the possibility of combining image-based features with the conventional brain networks.

Table 1. Summary of GCNs in radiologic image analysis

Method	Category	Input	Graph Construction		
			Node	Edge	Node/Edge Attributes
69	Single-modality	Task-fMRI	ROIs	Region-to-region correlations (threshold edges under 95% partial correlation)	Node: hand-craft features Edge: values of Pearson correlation and partial correlation between nodes.
54	Single-modality	fMRI	ROIs	Spatial graph: a KNN graph based on spatial coordinates of the ROI.	Rows/column of the functional connectivity matrix
				Functional graph: a KNN graph using the correlation distance between all ROI pairs.	
70	Single-modality	fMRI	ROIs	Edge-set	Node: Pearson correlation coefficient among nodes. Edge: Partial correlation coefficient among nodes.
74	Single-modality	rs- fMRI	Spatio graph: ROIs at the same time point.	Spatio graph: connect all nodes at the same time point.	Node: the average BOLD signal of the ROI i at time point t . Edge(Spatial graph): the functional affinity between ROIs. The functional affinity is calculated by the magnitude of correlation between the concatenated average BOLD time series.
			Temporal graph: the same ROI at the different time points.	Temporal graph: connect the corresponding node to the node of the same ROI at	

				the proceeding time point.	
75, 76	Single-modality	fMRI	Brain regions	Edge-set	Node: the BOLD signal at the entire time series. Edge: the statistical correlation of BOLD signals between the regions
55	Single-modality	DWI	ROIs	whole-brain probabilistic tractography algorithm	Rows/column of the connectivity matrix
81	Single-modality	DMRI	Points on manifold	Constructing the edge between two nodes when edge weights are larger than 0.	In q-space using two Gaussian kernels, accounting for differences in gradient directions and diffusion weighting
90	Single-modality	CT images	The connectivity of voxels	The voxels on the skeletons	Extracted by CNN model
92	Single-modality	CT images	1. The whole segmented airway region 2. the detected landmark positions	1. (internal) the connectivity between nodes and their KNN neighbors in Euclidean space. 2.(external) the airway structural prior information to connect two types of nodes.	Extracted by CNN model
93	Single-modality	CT images	The segmented	The airway structure.	Node: the anatomical airway structure and CNN extracted

			airway region		image features
94	Single-modality	RTCT and PET images	GTV _{LN} candidate	Euclidean distance among the boundary voxels of the tumor mask.	Node: extracted by CNN model
95	Single-modality	CBCT images	Landmark	The edge between landmarks is determined by whether the two landmarks are in the same anatomical regions	Node: extracted by CNN model
99	Single-modality	CT images	The slice of CT image	Densely connected graph	<p>Node: Extracted by CNN model and wavelet decomposition extraction.</p> <p>Edge: Cosine similarity among node features.</p>
82	Multi-modality	fMRI and sMRI	ROIs	Densely connected graph	Node: seven anatomical features and four functional connectivity statistic features.
					Edge: the Pearson correlation-induced similarity.
83	Multi-modality	fMRI and DTI	ROIs	Region-to-region correlations	Rows/column of connectivity matrix
84	Multi-modality	rs-fMRI and dMRI	ROIs	Edge set	<p>Edge (functional brain network): correlation of fMRI signals between nodes.</p> <p>Edge (structural brain network): probability of fiber tractography between nodes.</p>

86, 87	Multi-modality	T1WI and T2WI	A group of features in the partial region of the original regular grid coordinates.	Fully-connected graph	Node: extracted by CNN model
11	Multi-modality	fMRI and clinical data	ROIs	Connectivity the vertices	Node: image features
					Edge: non-image information
88	Multi-modality	rs-fMRI, DTI, gender, and age.	Each subjects (images)	The similarity between the node features and incorporates the phenotypic information.	Node: the concatenated local weighted clustering coefficient features from functional and structural connectivity.
89	Multi-modality	rs-fMRI, DTI, gender, and acquisition equipment.	Each subjects (images)	1. The similarity between the node features and incorporates the phenotypic information. 2. Connected nodes that belong to the same receptive field.	Node: the recursive feature elimination extracted features from functional and structural connectivity.
56	Multi-modality	X-ray images and meta-data	Image(patient)	Non-image meta-data	Extracted features by CNN.
97	Multi-modality	CT And non-image	ROIs	Fully connected graph	The concatenation feature consists of CNN extracted features and non-imaging

		data			clinical information.
91	Multi-modality	CT And X-ray images	Pixel	The neighborhood relationship between pixels	Grayscale intensity of the pixel

3.2. Histopathological image analysis

The growth of digitalized histopathological images presents a valuable resource to support rapid and accurate clinical decision making. The high-resolution whole slide image (WSI) contains rich tissue characteristics including patterns of cell nuclei, glands, and lymphocytes^{100,101}. Extensive pathological characteristics of tissue and cell interactions can be evidently observed that are not available in other clinical image data. For instance, lymphocytic infiltration of cancer status can be deduced only from histopathology imagery¹⁰². These pathological patterns can be used to build the biological graph networks that can inform disease status and thus discern predictive imaging biomarkers. Overall, we recognize that GCNs analysis is uniquely positioned to address key issues of histopathological applications, including data annotation, tissue connections, global-local information diagnostic fusion, and model prediction performance in challenging settings.

Developments of GCNs have brought remarkable advances into computational histopathology including label efficiency and multi-scale context representation. First, graph structure provides a reasonable choice to represent the entire slide in terms of tissue content connectivity. Such entire-slide graph representation can avoid fine-grained patch-wise label annotation. Since we know that patch-level labeling is highly time-intensive, even impossible, to include all ranges of tumor patches annotated by human experts. Second, graph structural representation can capture multi-scale contexts considering both global and local image-wise features towards enhanced prediction of disease outcomes. Third, graph structural representation builds upon the interaction among spatially-separated tiles that enables a more flexible and comprehensive receptive field. Such advances are analogous to the workflow of human experts that we consider tumor environment, tissue contents, and their interactions, rather than single tumor tiles, to diagnose tissue status of patients.

Because the high-resolution histopathological image does not present a natural form of graph structure, efficient graph representation becomes a vital factor for model development and optimization. Current graph construction in histopathology can be broadly categorized into patch-based and cell-based methods. First, patch-based graph construction methods aim to enable information extraction by considering the entire micro-environment (e.g., the cells and tissues), where comprehensive tissue micro-environment and cell dynamics

can be captured. In these patch-based methods, graph nodes are defined as the selected patches determined by ROIs in the histopathological image. The associated node attributes can be extracted by standard feature extractors (e.g., ResNet18 or VGG16). Graph edges are defined as the connectivity between nodes, which is determined by the feature or coordinate distance between two nodes. A smaller distance means a higher probability of connectivity. The connectivity between nodes could determine an adjacency matrix to represent the entire topological structure of the graph. Although the definition of primitive graph components (e.g., node and edge) are conceptually similar, most patch-based graph construction methods have different settings for node attributes and edge construction. As opposed to the patch-based graphs, cell-based graph methods emphasize the possible biological significance derived from histopathology. Cell-based graph construction methods aim to model the relationship between different cells and the micro-environment (e.g., tissues or vessels) utilizing graph-based features¹⁰³. In a cell graph, the detected and segmented nuclei or cell clusters are considered as nodes. The node attribute is defined as the combination of image-wised features, such as features extracted by CNN models, and the hand-crafted feature, such as the number or the size of nuclei, the average RGB value of nucleus, gray level co-occurrence matrix features, VGG19 features, and the number of neighbors of a nucleus¹⁰⁴. According to the assumption that adjacent cells are more likely to interact¹⁰³, the edge between the nodes can be determined via Delaunay triangulation¹⁰⁵ or the K-nearest-neighbour method¹⁰⁶, which could evaluate whether two cells (nodes) belong to the same cluster. The cells in the same cluster are more likely to have an edge between them. Despite a good performance on clinical classification tasks, these approaches cannot work well in capturing the diagnostic and prognostic information from the surrounding micro-environments (e.g., tissues and vessels). Meanwhile, constructing cell-centered graphs highly depends on cell detection accuracy. It is notable that constructing a cell-based graph and subsequent graph computing need an excessive computational complexity. The process of utilizing GCNs in histopathological image analysis is shown in Fig. 4. We outline several areas of clinical interest for GCNs in histopathology below.

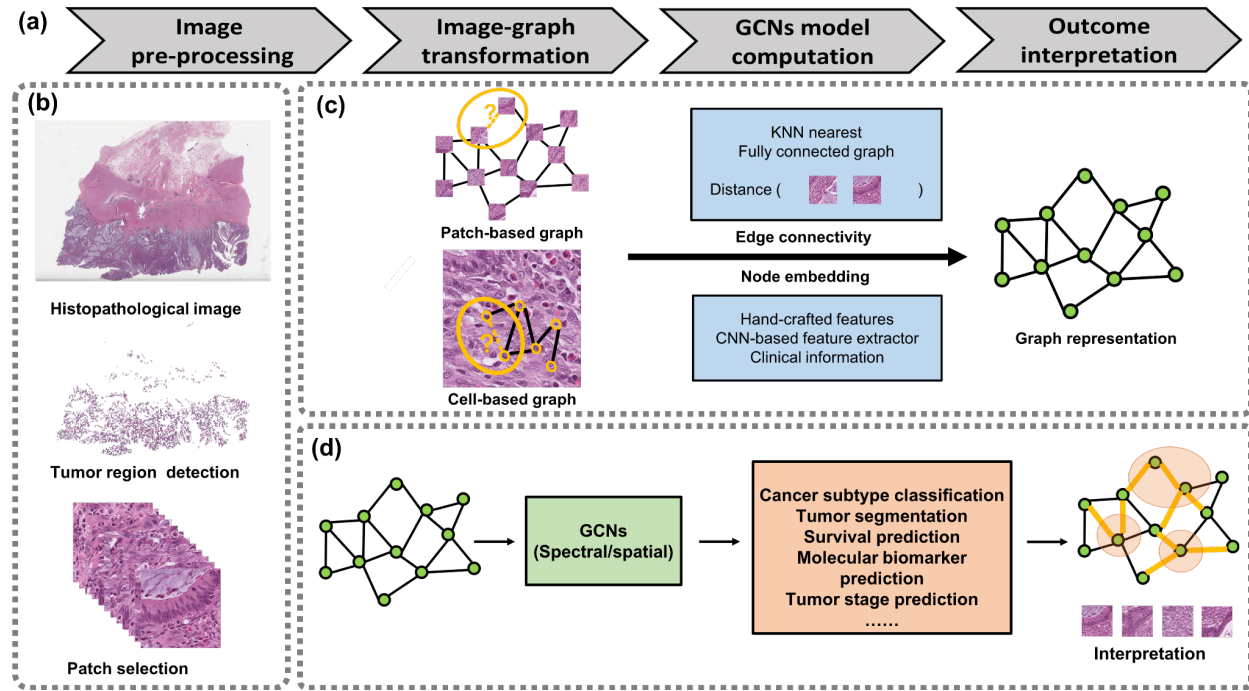


Fig 4. The illustration of the computational framework of GCNs in histopathological imagery. (a) Overall steps of image-based graph convolutional network framework. (b) Image preprocessing. The high-resolution images are normally split into manageable small-sized tumor tiles. We primarily focus on tumor tile processing and analysis for GCN development. **(c) Image-based graph transformation.** The transformation between image and graph-structured data is vital according to different tasks. Both patch-based and cell-based graphs can be established for downstream tasks. **(d) GCNs computation and outcome interpretation.** The inputs of GCNs are the constructed image-based graphs. The outcome interpretation of GCNs includes both node- and edge-wise findings to enable a multi-dimensional interpretation of outcomes.

3.2.1 Tumor segmentation

Accurate tumor segmentation in histopathology is designed to assist pathologists for improving workflow efficiency of clinical diagnosis⁷. Graph-based segmentation approaches can incorporate both local and global inter-tissue-region relations to build contextualized segmentation and thus improve the overall performance. For example, *SEGGINI* performs semantic segmentation of images by constructing tissue-graph representation and performing weakly-supervised segmentation via node classification by using weak multiplex annotations, i.e., inexact and incomplete annotations, in prostate cancer⁷. In this study, they defined graph nodes by superpixels merging based on channel-wise color similarity of superpixels at higher magnification. The node attribute is determined by the spatial and morphological features of the merged node (e.g., the merged superpixel). The spatial feature is computed by normalizing superpixel centroids by the image size and the morphological feature is extracted by a pre-trained MobileNetV2¹⁰⁷. They defined the edges by constructing a region adjacency graph (RAG)¹⁰⁸ from the spatial connectivity of superpixels. The local and global connection

of tissue details creates an alternative avenue for pixel-level segmentation evaluation that draws a contrast to other conventional convolutional-based tumor segmentation approaches^{109, 110, 111}. Another study¹¹² proposed an end-to-end framework that utilizes an unsupervised pretrained CNN to extract tile features and generate dynamics superpixels for graph construction, while using GCN for predicting the final segmentation map. In this study, the dynamics superpixels can be viewed as a key bridge between CNN and the GCN model, which are generated according to the CNN feature extraction.

3.2.2 Cancer tissue classification

Cancer subtype classification is crucial in clinical image analysis that can impact patient stratification, outcome assessment, and treatment development^{6, 113}. GCNs have been extensively studied in cancer subtype classification due to their unique ability to explore the relational features among tissue sub-regions (e.g., patches or cells). Patch-based graph construction approaches are intuitive to build a bridge between image features and graph structure. Conceptually, patches are defined as nodes and node attributes are extracted patch features, including CNN-based extracted and hand-crafted features. The edges are typically determined by the Euclidean distance of nodes. For example, the combination of ChebNet¹⁴ and GraphSage²⁰ presents its usefulness for classifying lung cancer subtypes in histopathological images⁶ via patch selection. All patches in the tissue region are grouped into multiple classes, and a portion of all clustered patches (e.g., 10%) are randomly selected within each class. Also, a simplified graph construction process⁶ can be useful to leverage all patch information. The global context among patches is considered while using a fully connected graph to represent the connection among nodes. Global pooling layers (e.g., global attention, max, and sum poolings) are able to generate graph representations for analyzing cancer classification. In particular, global attention pooling³⁶ provides strong interpretability to determine which nodes are relevant to the current graph-level classification tasks. In colorectal cancer histopathology, ChebNet¹⁴ shows its predictive power in lymph node metastasis (LNM) prediction¹¹³. Interestingly, a combination model of a variational autoencoder and generative adversarial network (VAE-GAN)¹¹⁴ is utilized to train as a feature extractor to decode the latent representations closer to their original data space. Further, the pixel-based graph construction could be understood as a variant of patch-based approaches. The study¹¹⁵ developed a group quadratic graph convolutional network for breast tissue and grade classification on pixel-based graph representation. The proposed model reduces the redundant node (e.g., pixel) feature, selects superior fusion feature, and enhances the representation ability of the graph convolutional unit by the pixel-based graph analysis.

As opposed to patch-based approaches, cell-based graph construction is under a key assumption that cell-cell interactions are the most salient points of information¹¹⁶. A common example is to define the detected nuclei as nodes¹⁰⁴ and while the overall node attributes are aggregated by concatenating multiple types of features (see Table2). The graph edge is determined by thresholding the Euclidean distance between nodes. In addition, the cell graph convolutional network¹⁰³ presents a generalized framework for grading colorectal cancer

histopathological images based on the combination of GraphSage²⁰, JK-Net⁴⁷, and Diffpooling³⁸. The edge between two nuclei is determined by a fixed distance while the maximum degree of each node is set to k corresponding to its k -nearest neighbors. Sharing a similar cell-graph construction strategy and graph component definition with¹⁰³, a GIN-based²¹ framework is designed for breast cancer subtype classification¹¹⁷. In addition, the clinical interpretation is provided by a cell-graph explainer that is inspired by a previous graph explainer¹¹⁸, a post-hoc interpretability method based on graph pruning optimization. The cell-graph explainer is able to prune the redundant graph components, such as the nodes that could not provide enough information in the decision making, and define the resulting subgraph as the explanation. Another cell graph application of cancer classification¹¹⁹ is built on top of robust spatial filtering (RSF)³², where RSF combined with attention mechanisms to rank the graph vertices in their relative order of importance, providing visualizable results on breast cancer and prostate cancer classification.

To leverage the advantages of patch- and cell-based graphs simultaneously, the model integration can provide additional auxiliary benefits by capturing detailed nuclei and micro-environment tissue information. A hierarchical cell-to-tissue graph neural network (HACT-Net)¹²⁰ is an example to consist of a low-level cell-based graph (e.g., cell-graph), a high-level patch-based graph (e.g., tissue-graph), and a hierarchical-cell-to-tissue representation for breast carcinoma subtype classification. For the cell-based graph, they defined nuclei as graph nodes that are detected by the pre-trained Hover-Net^{50, 121, 122}. For the patch-based graph, they determined graph nodes and their attributes by creating non-overlapping homogeneous superpixels and their features. The edges are constructed by a region adjacency graph¹⁰⁸ using the spatial centroids of the superpixels. Overall, such a joint analysis across histopathological scales leads to enhanced performance for cancer subtype classification.

Cancer staging and grade classification is also of clinical significance that comprises tumor tissue and nodal (e.g., tumor and lymph nodes) staging¹¹⁶. Patch-based graph construction strategy is commonly used in tumor staging classification in terms of graph attention⁸. Also, graph topological feature extraction is useful in colon cancer tumor stage prediction with well interpretation¹¹⁶. In particular, they utilized the Mapper¹²³ to project high-dimensional graph representation to a lower-dimensional space, summarizing higher-order architectural relationships between patch-level histological information to provide more favorable interpretations for histopathologists. Further, for liver fibrosis stage classification, the study¹²⁴ proposed a patch-based graph structure together with the GCN attention layer to analyze the spatial organization of the fibrosis patterns. They use the KNN algorithm to cluster the tiles to select regions of high collagen content as the centroid node for graph construction. The proposed pipeline allows for the separation of fibers in the slide into localized fibrosis patterns and the individual regions can be inspected by a pathologist¹²⁴. Also, cell-based graph construction strategy is useful for cancer grade classification. For example, for prostate cancer grade classification¹²⁵ in tissue micro-array, GraphSage²⁰ learns the global distribution of cell nuclei, cell morphometry, and spatial features without requiring pixel-level annotation. In this study, the cell nuclei are the node of the graph while

the three types of features consist of the node attribute, including the morphological feature (e.g., the area, roundness, eccentricity, convexity, orientation for each of the nucleus.), texture feature (e.g., the dissimilarity, homogeneity, energy, and ASM based on the obtained grey level co-occurrence matrix), and contrastive predictive coding features.

3.2.3 Survival prediction

Survival analysis is a long-standing clinical task to determine the prognostic likelihood of patients^{113, 126}. Both cell- and patch-based approaches can be considered to capture survival sensitive information of patients. For instance, the graph convolutional neural network with attention learning has shown to achieve a good performance on the survival prediction in colorectal cancer¹²⁷. Tumor tiles are defined as nodes and node attributes are extracted by the VGG16. Graph edges are constructed by thresholding the Euclidean distances between node attributes. After constructing the graph, they used the ChebNet¹⁴ framework for survival analysis on the histopathological images. With a similar definition of graph components, another study¹²⁸ designed a patch-based graph construction strategy in the Euclidean space. They utilized the DeepGCN⁹⁵ and global attention layer to boost the survival prediction performance and provided the interpretability across five cancer types. An integrated framework¹²⁹ extracted morphological features from histology images using CNNs and from the constructed cell-based graph using GraphSage²⁰, and also genomic (mutations, CNV, RNA-Seq) features using SNNs. A fusion of these deep features using the Kronecker Product is of great interest for accurate survival outcome prediction. In addition, cell-based and patch-based graphs can be further unified to allow a trade-off between efficiency and granularity¹³⁰. They used GAT or prostate cancer survival prediction using WSIs. Notably, a self-supervised learning method is proposed to pretrain the model, yielding improved performance over trained-from-scratch counterparts. For cell-based graphs, they use a Mask R-CNN¹³¹ for nuclei segmentation and define an eight-pixel width of the ring-like neighborhood region around each nucleus as its cytoplasm area. The nuclear morphometry features and visual texture features (intensity, gradient, and Haralick features) have made substantial contributions for both nuclear and cytoplasm region representations respectively. Despite these advances, uncertainty remains for exploring definitive roles of cell-level and patch-level characteristics with regard to overall survival likelihood of patients.

3.2.4 Molecular biomarker prediction

Image-based molecular biomarker prediction is promising to deepen our understanding of cancer biology across data modalities. Enormous efforts are gaining momentum to explore multiple image-to-genome associations in cancer research^{132, 133, 134}. The feature-enhanced graph network (FENet)¹² leverages histopathological-based graph structure to predict key molecular outcomes in colon cancer. Through the

spatial measurement of tumor patches, the image-to-graph transformation illustrates its unique value in predicting key genetic mutations. In particular, the use of GIN²¹ layer and jumping knowledge structure are useful to aggregate and update the patch embedding information. Alternatively, the cell-based construction method is considerable for cancer biomarker prediction¹³⁵. HoverNet¹²² is a popular choice for nuclei segmentation to support cell graph construction. Next, the agglomerative clustering¹³⁶ is utilized to group spatially neighboring nuclei into clusters. These clusters can be defined as graph nodes and the node attribute is determined by the standard deviation of nuclei sizes. Meanwhile the edges are constructed by using Delauney triangulation based on the geometric coordinates of cluster centers with a maximum distance connectivity threshold. Both cell- and patch-based approaches contribute to the integration of histopathology and genome as more biological data become accessible. We recognize that graph-based models can offer an efficient means to measure the cross-modality differences, which requires careful inputs on graph construction, model layer architectures, proper design of feature extraction for achieving improved performance of molecular outcome prediction.

Overall, Table 2 summarizes the category, type of tasks, and the graph-structure construction strategies. In this chapter, we have discussed novel perspectives for computational histopathological image analysis. In particular, GCNs-based methods provide a novel perspective to consider tumor heterogeneity in histopathological image analysis. Despite multiple challenges, the evolving capacity of current graph construction strategies (edge, node, and node attributes) makes it possible to address a variety of clinical tasks using histopathological images.

Table 2. Summary of GCNs in histopathological image analysis

Method	Category	Tasks	Graph Construction		
			Node	Edge	Node Attribute
7	Patch-based	Segmentation	Superpixel	Region adjacency graph	1. Normalizing superpixel centroids by image size 2. Extracted by a pre-trained MobileNetV2
112	Patch-based	Segmentation	Superpixel	The spatial adjacent neighbors	Node: Extracted features by fully-convolutional network. Edge: The similarity between statistical

					histogram features.
113	Patch-based	LNM prediction	Image Patch	Euclidean distance of node attributes	Extracted features of images patch and closer the feature space to the original one by VAE-GAN
6	Patch-based	Cancer Type/subtype classification	Image Patch	Fully connected graph attribute	Extracted features of images patch by DenseNet
116	Patch-based	Tumor Stage Prediction	Image Patch	The relationship between nodes	Extracted features of images patch
8	Patch-based	Tumour Node Metastasis (TNM) staging Prediction	Image Patch	The connectivity between nodes and their KNN neighbors in a fixed threshold	Texture feature extraction.
115	Pixel-based	Cancer tissue and grade classification	Pixel	The connectivity between nodes and their KNN neighbors	Extracted features by ResNet18.
124	Patch-based	Cancer tissue and grade classification	Patch	The connection between patch and the centroid node of each dense collagen region	Node: Extracted features by ResNet18. Edge: Encoded by the Euclidean distance from each tile to its corresponding centroid.
125	Cell-based	Tissue micro-arrays (TMA) Grade classification	Nuclei	The connectivity between nodes and their KNN neighbors	Morphological, texture, and contrastive predictive coding features.

104	Cell-based	Cancer Type/subtype classification	Nuclei	Thresholding the Euclidean distance between nuclei	Concatenating multiple types of features, including average RGB value, gray level co-occurrence matrix features, VGG19 features, and the number of neighbors of a nucleus.
103	Cell-based	Cancer Type/subtype classification	Nuclei	The connectivity between nodes and their KNN neighbors	16 hand-craft features and 17 nuclear descriptors
117	Cell-based	Cancer Type/subtype classification	Nuclei	Threshold the kNN graph by removing edges that are longer than a specified distance	16 hand-crafted features
119	Cell-based	Cancer Type/subtype classification	Nuclei	The Euclidean distance between nuclei	Concatenating edge and vertex features of a node
120	Patch-based	Cancer subtype classification	Superpixel	Region adjacency graph	Features of superpixels
	Cell-based		Nuclei	The connectivity between nodes and their KNN neighbors	Hand-craft features
127	Patch-based	Survival prediction	Image Patch	Euclidean distances between node attributes.	Extracted features of images patch by VGG16
128	Patch-based	Survival prediction	Image Patch	Euclidean distances between node coordinates.	Extracted features of images patch by ResNet50.
129	cell-based	Survival prediction	Nuclei	The connectivity between nodes and their KNN	Hand-craft and contrastive predictive

				neighbors	coding features.
130	Patch-based	Survival prediction	patch	The connectivity between nodes and their KNN neighbors (K=5)	Image features and cell-based graph representation
	cell-based		Nuclei	The connectivity between nodes and its KNN neighbors (K =3)	Nuclear morphometry features and imaging features (including intensity, gradient and Haralick features)
12	Patch-based	Biomarker Prediction	Image Patch	Thresholding the Euclidean distance between node coordinates	Extracted features of images patch by ResNet18
135	Cell-based	Biomarker prediction	The geometric center of nuclei cluster	Delauney triangulation between cluster center with a maximum distance threshold	The count of the six nuclei types and the standard deviation of nuclear sizes

4. Other image-based applications

GCNs have demonstrated their analytical ability in alternative medical image disciplines to facilitate structural analysis of disease diagnosis (e.g., eye disease and skin lesion), surgery scene understanding, and Bone Age Assessment. For instance, GCNs have been studied in dermatology and eye-related diseases, involving retinal, fundus, and fluorescein angiography (FA) images^{126,137, 138, 139}. Similar to radiological and histopathological images, patch-based graph construction strategies are widely used in the above image domains. GCNs have shown to be valuable to learn the vessel shape structures and local appearance for vessel segmentation in retinal images¹³⁷. Also, GCNs were applied to the artery and vein classification by using both fundus images and corresponding fluorescein angiography (FA) images¹³⁸. With a designed graph U-Nets architecture⁴⁰, the high-level connectivity of vascular structures can be learned from node clustering in the node pooling layers. In addition, a study¹⁴⁰ proposed a framework that combines the CNN and ResGCN⁸⁵ model to enhance the

segmentation performance of fetal head on ultrasound images. Furthermore, GCNs show their power in differential diagnosis of skin conditions using clinical images¹³⁹. This problem is formulated as a multi-label classification task over 80 conditions when only incomplete image labels are available. The label incompleteness is addressed by combining a classification network with a graph convolutional network that characterizes label co-occurrence¹³⁹. Each clinical image is defined as a graph node and the connectivity between two nodes is determined by domain knowledge of skin condition by board-certified dermatologists. It is noteworthy that edge connection is made by inputs from human experts that two dermatologists provide overlapped differential diagnoses groups and connect an edge when two labels appear in at least one differential group by both dermatologists. In addition, a cell-based graph analysis¹²⁶ combines multiple types of GCNs with graph poolings, including GIN^{20,21}, GraphSage²¹, and GCN¹⁶ for survival prediction of gastric cancer using immunohistochemistry (mIHC) images. The graph nodes are determined by six antibodies of PanCK, CD8, CD68, CD163, Foxp3, and PD-L1, which were used as annotation indicators for six different types of cells. The node attributes are determined by cell locations, types, and morphological features. The edges are constructed by the maximum effective distance between immune and tumor cells, which is equivalent to 40 pixels in the magnification of this study. Furthermore, a surgery scene graph analysis¹⁴¹ utilized GraphSage to predict surgical interactions between instruments and surgical regions of interest. In addition, GCNs provide the potential for automatic bone age assessment and ROI score prediction on hand radiograph¹⁴². This study proposed an anatomy-based group convolution block to predict the ROI scores by processing the local features of ROIs. Also, they presented a dual graph-based attention module to compute the patient-specific attention and context attention for ROI score prediction.

Table 3. Summary of GCNs in other image analysis

Method	Image type	Tasks	Graph Construction		
			Node	Edge	Node/edge Attribute
126	Immunohistoc hemistry (mIHC) images	Survival prediction	Cell	Euclidean distances between nodes.	<p>Node: the cell locations, optical features of stained cells, and morphology features</p> <p>Edge:</p> $\frac{40}{\text{distance between cells}}$ <p>(set to 0 while no</p>

					interaction between nodes)
137	Retinal image	Vessel Segmentation	Pixels with maximum vessel probability	Geodesic distance between nodes (smaller than a fixed threshold)	Extracted by CNN.
138	Fundus images and corresponding fluorescein angiography (FA) images	The artery and vein classification	Vessel pixels with in NxN local patches	Edges are con- structed with existing vessel pixels within an $N \times N$ local patch.	Extracted by graph U-nets.
140	Fundus images and ultrasound images	Optic disc and cup segmentation (fundus images) Fetal head segmentation (ultrasound images)	The object boundaries are divided into N vertices with the same interval.	Every two consecutive vertices on the boundary and the center vertex are connected to form a triangle.	Nodes: Extracted by CNN.
139	Skin clinical images	Skin condition classification	Image	Connected an edge when two labels appear in at least one differential group by both dermatologists.	Node: Extracted by CNN Edge: $\frac{C(i, j)}{C(i) + C(j)}$ $C(i, j)$: the number of images have two label at same time $C(i)/C(j)$: the number of images in class i/j.
141	Surgery scene images	Surgery scene understanding	Surgical tools and defective	Interactions between nodes	Node and edge: CNN extracted

			tissues		features with label smoothing
142	Hand radiograph	Bone age assessment	ROIs	1. The natural connections among ROIs. 2. The full connections among the ROIs in the same anatomy group.	Node: ROI features.

5. Discussion and future direction

The rapid growth of GCNs^{12, 113, 127} and their extensions have been increasingly utilized for processing, integrating, and analyzing multi-modality medical imaging and other types of biological data. We here discuss several future research directions and common challenges to advance the research in medical image analysis and related research fields. We particularly outline key aspects of importance, including GCN model interpretation, the value of pre-training model, evaluation pipeline, large-scale benchmark, and emerging technical insights.

5.1 Interpretability

The interpretation of GCNs is of heightened interest to make the outcome understandable, ensure model validity, and enhance clinical relevance. In our focus, a well-designed interpretation framework of GCNs is expected to provide the explanation and visualization for both image-wise and graph components understanding. Such an interpretative ability can be highly attractive to clinicians in the process of diagnosing regions of interest in histopathology, enabling an understanding of spatial and regional interactions from graph structures¹². As demonstrated, three metrics are useful to design and understand the interpretation capability of GCNs¹⁴³: (1) Fidelity refers to the importance of classification as measured by the impact of node attributes, (2) Contrastively points to the significance with respect to different classes, and (3) Sparsity reflects the sparseness level on a graph. These metrics can help generate and measure the valuable heat maps of graph nodes given their attributes. Representative approaches include gradient class activation mapping (Grad-CAM), contrastive excitation backpropagation (c-EB), and contrastive gradient (CG)¹⁴⁴. Further, we recognize that emerging studies have explored the specified interpretation strategy for GCNs^{117, 118}. For instance, an ROI-

selection pooling layer (R-pool)¹⁴³ highlights the node importance for predicting neurological disorders by removing noisy nodes to realize a dimension reduction of the entire graph. Rather than node-level feature interpretation, additional efforts will be greatly needed on interpreting the relational information in graphs. GnnExplainer¹¹⁸ is an example to leverage the recursive neighborhood-aggregation scheme to identify graph pathways as well as node feature information passing along the edges. The design of GnnExplainer is appealing to visualize the detailed cell-graph structure and provide class-specific interpretation for breast cancer¹¹⁷. As a result, we strongly emphasize that the interpretation process considers an in-depth joint understanding of the clinical task, graph model architecture, and model performance.

5.2 Model pretraining

Pretraining GCNs aims to train a model on the tasks with a sufficient amount of data and labels and finetune the model into downstream tasks. Pre-trained GCNs can serve as a foundation model to improve the generalization power when the size of the training set is often limited in medical imaging¹⁴⁵. The pretraining workflow of GCNs typically includes the model training rules, hyper-parameter settings, and constructed-graph augmentation strategies. A key pretraining scheme for a graph-level task is to reconstruct the vertex adjacency information (e.g. GraphSAGE²¹) without hurting intrinsic structural information¹⁴⁶. We offer several compelling directions of pretraining strategy to improve GCNs model robustness and their utility in different tasks. First, the graph-wise augmentation strategies have a large room to facilitate the pretraining of graphs. For instance, the out-of-distribution samples can be analyzed via node-level and graph-level augmentations^{145, 146}. Second, exploring label-efficient models (e.g., unsupervised or self-supervised learning) in conjunction with pretraining strategies¹⁴⁶ could greatly alleviate the labeling shortage. Notable studies^{145, 146, 147} have achieved good performance in downstream tasks while leveraging the graph-based pretraining strategies. Considering the above directions, a self-supervised learning framework for GCNs pretraining¹⁴⁶ demonstrates that graph-wise augmentation strategies are useful to address the graph data heterogeneity. The pretraining is performed through maximizing the agreement between two augmented views of the same graph via performing node dropping, edge perturbation, attribute masking, and subgraph selection. Notably, only a small partition of graph components will be changed, meanwhile the semantic meaning of the graph has been preserved. Such a strategy brings graph data diversity that is greatly needed for building robust pre-trained GCN models. Taken together, the research on pretraining GCNs and their practical impact is only to start and will continue to make progress on downstream image-related clinical tasks.

5.3 Evaluation of graph construction strategies

The evaluation of graph construction in medical imaging is vital because the associated graph construction could significantly affect the model performance and the interpretation of outcomes. The general graph construction methods used ROIs (e.g., image patches or brain neurons) as graph nodes and the node attributes are obtained by standard feature extractors (e.g., ResNet18). In addition, edges represent the connections

between nodes which could be determined by the Euclidean distance between node features, or the connections between ROIs which are determined by patch coordinates or the actual neural fiber connections. Currently, graph construction strategies are applied in different tasks and a generalized graph construction evaluation strategy is not explicitly developed yet. It is even more difficult to determine which kind of graph construction is generalizable for task-specific medical image analysis because of various datasets and graph construction metrics. Also, developing a generalized graph construction evaluation strategy is necessary for GCNs to better process medical image data across multiple modalities because the model performance is highly related to the quality of constructed graph-structured data. The benchmarking framework^{148, 149} has rigorously evaluated the performance of graph neural networks on medium-scale datasets and demonstrates its usefulness for analyzing message-passing capability in GCNs. Also, a comparison strategy among multiple GCNs¹⁴⁹ can address the issues of reproducibility and replicability. Following the graph evaluation^{148, 149}, we need to define statistical distinctions to ensure the performance of GCNs. For example, it is helpful for model training and human understanding if the graph structure and feature distribution differences between positive and negative patient samples are significantly different.

5.4 Real-world large-scale graph benchmark

Despite the remarkable effort on standardization of medical imaging cohorts, the high-quality, large-scale graph-defined benchmark has not been readily available for AI model evaluation, especially in medical image analysis. Open Graph Benchmark (OGB) exemplifies the initiative that contains a diverse set of real-world benchmark datasets (e.g., protein, drug, and molecular elements) to facilitate scalable and reproducible graph machine learning research¹⁵⁰. The number of graphs and nodes in each graph are both massive in OGB. Even small-scale OGB graphs can have more than 100 thousand nodes or more than 1 million edges. This comprehensive dataset in various domains can be viewed as a baseline to support the GCNs' development and comparison. Related works have been explored on graphs including a chemistry dataset with 2 million graphs and a biology dataset with 395K graphs¹⁴⁵. As seen in OGB development, there are challenges to collecting and processing suitable medical image datasets and constructing meaningful graphs following the image-to-graph transformation. First, we need to collect a large number of medical images across multiple centers to ensure data diversity. It is also essential to provide detailed annotation information for collected datasets on the image-level region of interest. Second, graph-wise statistics is important to allow measurement of graph-level dynamics. Notable graph metrics¹⁵¹, such as the average node degree, clustering coefficient, closeness centrality, and betweenness centrality, can be used to assess graph characteristics and help determine unique graph structures. For instance, the average node degree calculates the average degree of the neighborhood of each node to delineate the connectivity between nodes to their neighbors. The clustering coefficient measures how many nodes in the graph tend to cluster together. Closeness centrality highlights nodes that can easily access other nodes. Third, we must carefully design image-graph components, such as the definition of graph nodes in different types of graphs that are vital to downstream clinical tasks. Finally, the real impact of pre-trained

foundation models on large-scale graph-wise datasets still needs to be explored. While using pretraining GCNs to improve data-efficiency issues in medical image analysis, the models can be well-trained on the large-scale graph-wise dataset and adapt into specific tasks, even with a limited size of downstream data.

5.5 Technological advancements

The rapid development of deep learning is bringing novel perspectives to address the challenges of graph-based image analysis. The transformer architecture²³, emphasizing the use of a self-attention mechanism to explore long-range sequential knowledge, emerges to improve the model performance in a variety of natural language processing (NLP)¹⁵² and computer vision tasks^{153, 154}. A graph-wise transformer can be effectively considered to capture both local and global contexts, thus holding the promise to overcome the limitation of spatial-temporal graph convolutions. For example, graph convolutional skeleton transformers integrate both dynamical attention and global context, as well as local topology structure in GCNs¹⁵⁵ while the spatial transformer attention module discovers the global correlations between the bone-connected and the approximated connected joints of graph topology. In medical image analysis, the combination of GCNs and transformer models can be favored to process 3D MRI sequences to boost the model prediction performance, where GCNs explore the topological features while Transformers could model the temporal relationship among MRI sequences. In the meantime, self-supervised learning strategy is emerging in graph-driven analysis with limited availability of imaging data. Notably, self-supervised learning (SSL) provides a means to pretrain a model with unlabeled data, followed by fine-tuning the model for a downstream task with limited annotations¹⁵⁶. Contrastive learning (CL), as a particular variant of SSL, introduces a contrastive loss to enforce representations to be close for similar pairs and far for dissimilar pairs^{156, 157}. Another technique to address the limitation of data labeling is the advent of self-training learning to generate pseudo-label for model retraining and optimization¹⁵⁸. A self-training method for MRI segmentation has shown the potential solution for cross-scanner and cross-center data analytical tasks¹⁵⁸. Also, the teacher-student framework is another type of self-training, which trains a good teacher model with labeled data to annotate the unlabeled data, and finally, the labeled data and data with pseudo-labels can jointly train a student model¹³¹. Overall, both self-supervised learning and self-training strategies can be utilized in GCNs model training to potentially improve the model performance and overcome the annotation and data scale challenges.

6. Conclusion

We have witnessed a growing trend of graph convolutional networks applied to medical image analysis over the past few years. The convergence of GCNs, medical imaging data, and other clinical data, brings advances into outcome interpretation, disease understanding, and novel insights into data-driven model assessment. These breakthroughs, together with data fusion ability, local and global feature inference, and model training efficiency, lead to a wide range of downstream applications across clinical imaging fields. Nevertheless, the

development of benchmark graph-based medical datasets is yet to be established. Consistency and validity of graph construction strategy in medical imaging are greatly needed in future research. Recent technological advances can be considered to enhance and optimize GCNs in addressing challenging problems. We hope that the gleaned insights of this review will serve as a guideline for researchers on graph-driven deep learning across medical imaging disciplines and will inspire continued efforts on data-driven biomedical research and healthcare applications.

Reference

1. Zhou J, et al. Graph neural networks: A review of methods and applications. *AI Open* **1**, 57-81 (2020).
2. Bruna J, Zaremba W, Szlam A, LeCun Y. Spectral networks and locally connected networks on graphs. *arXiv preprint arXiv:13126203*, (2013).
3. Wu Z, Pan S, Chen F, Long G, Zhang C, Philip SY. A comprehensive survey on graph neural networks. *IEEE transactions on neural networks and learning systems* **32**, 4-24 (2020).
4. Zhang S, Tong H, Xu J, Maciejewski R. Graph convolutional networks: a comprehensive review. *Computational Social Networks* **6**, 1-23 (2019).
5. Failmezger H, Muralidhar S, Rullan A, de Andrea CE, Sahai E, Yuan Y. Topological Tumor Graphs: a graph-based spatial model to infer stromal recruitment for immunosuppression in melanoma histology. *Cancer research* **80**, 1199-1209 (2020).
6. Adnan M, Kalra S, Tizhoosh HR. Representation learning of histopathology images using graph neural networks. In: *Proceedings of the IEEE/CVF Conference on Computer Vision and Pattern Recognition Workshops* (2020).
7. Anklin V, et al. Learning Whole-Slide Segmentation from Inexact and Incomplete Labels using Tissue Graphs. *arXiv preprint arXiv:210303129*, (2021).
8. Raju A, Yao J, Haq MM, Jonnagaddala J, Huang J. Graph attention multi-instance learning for accurate colorectal cancer staging. In: *International Conference on Medical Image Computing and Computer-Assisted Intervention*). Springer (2020).

9. Perozzi B, Al-Rfou R, Skiena S. Deepwalk: Online learning of social representations. In: *Proceedings of the 20th ACM SIGKDD international conference on Knowledge discovery and data mining*) (2014).
10. Grover A, Leskovec J. node2vec: Scalable feature learning for networks. In: *Proceedings of the 22nd ACM SIGKDD international conference on Knowledge discovery and data mining*) (2016).
11. Huang Y, Chung AC. Edge-variational graph convolutional networks for uncertainty-aware disease prediction. In: *International Conference on Medical Image Computing and Computer-Assisted Intervention*). Springer (2020).
12. Ding K, Liu Q, Lee E, Zhou M, Lu A, Zhang S. Feature-Enhanced Graph Networks for Genetic Mutational Prediction Using Histopathological Images in Colon Cancer. In: *International Conference on Medical Image Computing and Computer-Assisted Intervention*). Springer (2020).
13. Qu H, et al. Genetic mutation and biological pathway prediction based on whole slide images in breast carcinoma using deep learning. *NPJ precision oncology* **5**, 1-11 (2021).
14. Defferrard M, Bresson X, Vandergheynst P. Convolutional neural networks on graphs with fast localized spectral filtering. *Advances in neural information processing systems* **29**, 3844-3852 (2016).
15. Levie R, Monti F, Bresson X, Bronstein MM. Cayleynets: Graph convolutional neural networks with complex rational spectral filters. *IEEE Transactions on Signal Processing* **67**, 97-109 (2018).
16. Kipf TN, Welling M. Semi-supervised classification with graph convolutional networks. *arXiv preprint arXiv:160902907*, (2016).
17. Li R, Wang S, Zhu F, Huang J. Adaptive graph convolutional neural networks. In: *Proceedings of the AAAI Conference on Artificial Intelligence*) (2018).
18. Zhuang C, Ma Q. Dual graph convolutional networks for graph-based semi-supervised classification. In: *Proceedings of the 2018 World Wide Web Conference*) (2018).
19. Gilmer J, Schoenholz SS, Riley PF, Vinyals O, Dahl GE. Neural message passing for quantum chemistry. In: *International conference on machine learning*). PMLR (2017).
20. Hamilton WL, Ying R, Leskovec J. Inductive representation learning on large graphs. In: *Proceedings of the 31st International Conference on Neural Information Processing Systems*) (2017).
21. Xu K, Hu W, Leskovec J, Jegelka S. How powerful are graph neural networks? *arXiv preprint arXiv:181000826*, (2018).
22. Veličković P, Cucurull G, Casanova A, Romero A, Lio P, Bengio Y. Graph attention networks. *arXiv preprint arXiv:171010903*, (2017).

23. Vaswani A, *et al.* Attention is all you need. In: *Advances in neural information processing systems* (2017).
24. Scarselli F, Gori M, Tsoi AC, Hagenbuchner M, Monfardini G. The graph neural network model. *IEEE transactions on neural networks* **20**, 61-80 (2008).
25. Liu M, Gao H, Ji S. Towards deeper graph neural networks. In: *Proceedings of the 26th ACM SIGKDD International Conference on Knowledge Discovery & Data Mining* (2020).
26. Kearnes S, McCloskey K, Berndl M, Pande V, Riley P. Molecular graph convolutions: moving beyond fingerprints. *Journal of computer-aided molecular design* **30**, 595-608 (2016).
27. Pham T, Tran T, Phung D, Venkatesh S. Column networks for collective classification. In: *Thirty-first AAAI conference on artificial intelligence* (2017).
28. Simonovsky M, Komodakis N. Dynamic edge-conditioned filters in convolutional neural networks on graphs. In: *Proceedings of the IEEE conference on computer vision and pattern recognition* (2017).
29. Atwood J, Towsley D. Diffusion-convolutional neural networks. In: *Advances in neural information processing systems* (2016).
30. Li Y, Yu R, Shahabi C, Liu Y. Diffusion convolutional recurrent neural network: Data-driven traffic forecasting. *arXiv preprint arXiv:170701926*, (2017).
31. Derr T, Ma Y, Tang J. Signed graph convolutional networks. In: *2018 IEEE International Conference on Data Mining (ICDM)*). IEEE (2018).
32. Such FP, *et al.* Robust spatial filtering with graph convolutional neural networks. *IEEE Journal of Selected Topics in Signal Processing* **11**, 884-896 (2017).
33. Wang X, *et al.* Heterogeneous graph attention network. In: *The World Wide Web Conference* (2019).
34. Mesquita D, Souza AH, Kaski S. Rethinking pooling in graph neural networks. *arXiv preprint arXiv:201011418*, (2020).
35. Zhang M, Cui Z, Neumann M, Chen Y. An end-to-end deep learning architecture for graph classification. In: *Thirty-Second AAAI Conference on Artificial Intelligence* (2018).
36. Li Y, Tarlow D, Brockschmidt M, Zemel R. Gated graph sequence neural networks. *arXiv preprint arXiv:151105493*, (2015).
37. Bianchi FM, Grattarola D, Alippi C. Mincut pooling in graph neural networks. (2019).
38. Ying R, You J, Morris C, Ren X, Hamilton WL, Leskovec J. Hierarchical graph representation learning with differentiable pooling. *arXiv preprint arXiv:180608804*, (2018).
39. Cangea C, Veličković P, Jovanović N, Kipf T, Liò P. Towards sparse hierarchical graph classifiers. *arXiv preprint arXiv:181101287*, (2018).

40. Gao H, Ji S. Graph u-nets. In: *international conference on machine learning*). PMLR (2019).
41. Knyazev B, Taylor GW, Amer MR. Understanding attention and generalization in graph neural networks. *arXiv preprint arXiv:190502850*, (2019).
42. Lee J, Lee I, Kang J. Self-attention graph pooling. In: *International Conference on Machine Learning*). PMLR (2019).
43. Diehl F, Brunner T, Le MT, Knoll A. Towards graph pooling by edge contraction. In: *ICML 2019 Workshop on Learning and Reasoning with Graph-Structured Data*) (2019).
44. Diehl F. Edge contraction pooling for graph neural networks. *arXiv preprint arXiv:190510990*, (2019).
45. Chen D, Lin Y, Li W, Li P, Zhou J, Sun X. Measuring and relieving the over-smoothing problem for graph neural networks from the topological view. In: *Proceedings of the AAAI Conference on Artificial Intelligence*) (2020).
46. Li Q, Han Z, Wu X-M. Deeper insights into graph convolutional networks for semi-supervised learning. In: *Thirty-Second AAAI conference on artificial intelligence*) (2018).
47. Xu K, Li C, Tian Y, Sonobe T, Kawarabayashi K-i, Jegelka S. Representation learning on graphs with jumping knowledge networks. In: *International Conference on Machine Learning*). PMLR (2018).
48. Ibragimov B, Xing L. Segmentation of organs - at - risks in head and neck CT images using convolutional neural networks. *Medical physics* **44**, 547-557 (2017).
49. Havaei M, *et al*. Brain tumor segmentation with deep neural networks. *Medical image analysis* **35**, 18-31 (2017).
50. Chilamkurthy S, *et al*. Deep learning algorithms for detection of critical findings in head CT scans: a retrospective study. *The Lancet* **392**, 2388-2396 (2018).
51. Grewal M, Srivastava MM, Kumar P, Varadarajan S. Radnet: Radiologist level accuracy using deep learning for hemorrhage detection in ct scans. In: *2018 IEEE 15th International Symposium on Biomedical Imaging (ISBI 2018)*). IEEE (2018).
52. Lakshmanaprabu S, Mohanty SN, Shankar K, Arunkumar N, Ramirez G. Optimal deep learning model for classification of lung cancer on CT images. *Future Generation Computer Systems* **92**, 374-382 (2019).
53. Frid-Adar M, Klang E, Amitai M, Goldberger J, Greenspan H. Synthetic data augmentation using GAN for improved liver lesion classification. In: *2018 IEEE 15th international symposium on biomedical imaging (ISBI 2018)*). IEEE (2018).
54. Ktena SI, *et al*. Metric learning with spectral graph convolutions on brain connectivity networks. *NeuroImage* **169**, 431-442 (2018).

55. Zhang Y, Zhan L, Cai W, Thompson P, Huang H. Integrating heterogeneous brain networks for predicting brain disease conditions. In: *International Conference on Medical Image Computing and Computer-Assisted Intervention*). Springer (2019).
56. Burwinkel H, *et al.* Adaptive image-feature learning for disease classification using inductive graph networks. In: *International Conference on Medical Image Computing and Computer-Assisted Intervention*). Springer (2019).
57. Kong Y, Gao J, Xu Y, Pan Y, Wang J, Liu J. Classification of autism spectrum disorder by combining brain connectivity and deep neural network classifier. *Neurocomputing* **324**, 63-68 (2019).
58. Logothetis NK, Pauls J, Augath M, Trinath T, Oeltermann A. Neurophysiological investigation of the basis of the fMRI signal. *nature* **412**, 150-157 (2001).
59. Seeman P, Madras B. *Imaging of the human brain in health and disease*. Elsevier (2013).
60. Narayan R. *Encyclopedia of biomedical engineering*. Elsevier (2018).
61. Korolev S, Safiullin A, Belyaev M, Dodonova Y. Residual and plain convolutional neural networks for 3D brain MRI classification. In: *2017 IEEE 14th international symposium on biomedical imaging (ISBI 2017)*). IEEE (2017).
62. Sporns O. Contributions and challenges for network models in cognitive neuroscience. *Nature neuroscience* **17**, 652-660 (2014).
63. Shen W, Zhou M, Yang F, Yang C, Tian J. Multi-scale convolutional neural networks for lung nodule classification. In: *International conference on information processing in medical imaging*). Springer (2015).
64. Shen W, *et al.* Multi-crop convolutional neural networks for lung nodule malignancy suspiciousness classification. *Pattern Recognition* **61**, 663-673 (2017).
65. Wang S, *et al.* Central focused convolutional neural networks: Developing a data-driven model for lung nodule segmentation. *Medical image analysis* **40**, 172-183 (2017).
66. Tzourio-Mazoyer N, *et al.* Automated anatomical labeling of activations in SPM using a macroscopic anatomical parcellation of the MNI MRI single-subject brain. *Neuroimage* **15**, 273-289 (2002).
67. Zalesky A, *et al.* Whole-brain anatomical networks: does the choice of nodes matter? *Neuroimage* **50**, 970-983 (2010).
68. Liu C, *et al.* Computational network biology: data, models, and applications. *Physics Reports* **846**, 1-66 (2020).
69. Li X, Dvornek NC, Zhou Y, Zhuang J, Ventola P, Duncan JS. Graph neural network for interpreting task-fMRI biomarkers. In: *International Conference on Medical Image Computing and Computer-Assisted Intervention*). Springer (2019).

70. Li X, *et al.* Pooling regularized graph neural network for fmri biomarker analysis. In: *International Conference on Medical Image Computing and Computer-Assisted Intervention*). Springer (2020).

71. Di Martino A, *et al.* The autism brain imaging data exchange: towards a large-scale evaluation of the intrinsic brain architecture in autism. *Molecular psychiatry* **19**, 659-667 (2014).

72. Sudlow C, *et al.* UK biobank: an open access resource for identifying the causes of a wide range of complex diseases of middle and old age. *PLoS medicine* **12**, e1001779 (2015).

73. Koch G, Zemel R, Salakhutdinov R. Siamese neural networks for one-shot image recognition. In: *ICML deep learning workshop*). Lille (2015).

74. Gadgil S, Zhao Q, Pfefferbaum A, Sullivan EV, Adeli E, Pohl KM. Spatio-temporal graph convolution for resting-state fmri analysis. In: *International Conference on Medical Image Computing and Computer-Assisted Intervention*). Springer (2020).

75. Lin Y, *et al.* Learning dynamic graph embeddings for accurate detection of cognitive state changes in functional brain networks. *NeuroImage* **230**, 117791 (2021).

76. Lin Y, Hou J, Laurienti PJ, Wu G. Detecting changes of functional connectivity by dynamic graph embedding learning. In: *International Conference on Medical Image Computing and Computer-Assisted Intervention*). Springer (2020).

77. Achard S, Salvador R, Whitcher B, Suckling J, Bullmore E. A resilient, low-frequency, small-world human brain functional network with highly connected association cortical hubs. *Journal of Neuroscience* **26**, 63-72 (2006).

78. van der Horn HJ, Liemburg EJ, Scheenen ME, de Koning ME, Spikman JM, van der Naalt J. Graph analysis of functional brain networks in patients with mild traumatic brain injury. *PLoS One* **12**, e0171031 (2017).

79. Kabbara A, Falou WE, Khalil M, Wendling F, Hassan M. Graph analysis of spontaneous brain network using EEG source connectivity. *arXiv preprint arXiv:160700952*, (2016).

80. Marek K, *et al.* The Parkinson progression marker initiative (PPMI). *Progress in neurobiology* **95**, 629-635 (2011).

81. Chen G, *et al.* Estimating Tissue Microstructure with Undersampled Diffusion Data via Graph Convolutional Neural Networks. In: *International Conference on Medical Image Computing and Computer-Assisted Intervention*). Springer (2020).

82. Yang H, *et al.* Interpretable multimodality embedding of cerebral cortex using attention graph network for identifying bipolar disorder. In: *International Conference on Medical Image Computing and Computer-Assisted Intervention*). Springer (2019).

83. Liu J, Ma G, Jiang F, Lu C-T, Philip SY, Ragin AB. Community-preserving graph convolutions for structural and functional joint embedding of brain networks. In: *2019 IEEE International Conference on Big Data (Big Data)*). IEEE (2019).

84. Zhang W, Zhan L, Thompson P, Wang Y. Deep representation learning for multimodal brain networks. In: *International Conference on Medical Image Computing and Computer-Assisted Intervention*). Springer (2020).
85. Li G, Muller M, Thabet A, Ghanem B. Deepgcns: Can gcns go as deep as cnns? In: *Proceedings of the IEEE/CVF international conference on computer vision*) (2019).
86. Mo S, et al. Multimodal priors guided segmentation of liver lesions in MRI using mutual information based graph co-attention networks. In: *International Conference on Medical Image Computing and Computer-Assisted Intervention*). Springer (2020).
87. Mo S, et al. Mutual Information-Based Graph Co-Attention Networks for Multimodal Prior-Guided Magnetic Resonance Imaging Segmentation. *IEEE Transactions on Circuits and Systems for Video Technology*, (2021).
88. Yu S, et al. Multi-scale enhanced graph convolutional network for early mild cognitive impairment detection. In: *International Conference on Medical Image Computing and Computer-Assisted Intervention*). Springer (2020).
89. Song X, Frangi A, Xiao X, Cao J, Wang T, Lei B. Integrating similarity awareness and adaptive calibration in graph convolution network to predict disease. In: *International Conference on Medical Image Computing and Computer-Assisted Intervention*). Springer (2020).
90. Zhai Z, et al. Linking convolutional neural networks with graph convolutional networks: application in pulmonary artery-vein separation. In: *International Workshop on Graph Learning in Medical Imaging*). Springer (2019).
91. Saha P, Mukherjee D, Singh PK, Ahmadian A, Ferrara M, Sarkar R. GraphCovidNet: A graph neural network based model for detecting COVID-19 from CT scans and X-rays of chest. *Scientific reports* **11**, (2021).
92. Tan Z, Feng J, Zhou J. SGNet: Structure-Aware Graph-Based Network for Airway Semantic Segmentation. In: *International Conference on Medical Image Computing and Computer-Assisted Intervention*). Springer (2021).
93. Zhao T, Yin Z. Airway Anomaly Detection by Prototype-Based Graph Neural Network. In: *International Conference on Medical Image Computing and Computer-Assisted Intervention*). Springer (2021).
94. Chao C-H, et al. Lymph node gross tumor volume detection in oncology imaging via relationship learning using graph neural network. In: *International Conference on Medical Image Computing and Computer-Assisted Intervention*). Springer (2020).
95. Lang Y, et al. Automatic localization of landmarks in craniomaxillofacial CBCT images using a local attention-based graph convolution network. In: *International Conference on Medical Image Computing and Computer-Assisted Intervention*). Springer (2020).
96. Rajpurkar P, et al. Chexnet: Radiologist-level pneumonia detection on chest x-rays with deep learning. *arXiv preprint arXiv:171105225*, (2017).

97. Cui H, et al. Co-graph Attention Reasoning Based Imaging and Clinical Features Integration for Lymph Node Metastasis Prediction. In: *International Conference on Medical Image Computing and Computer-Assisted Intervention*). Springer (2021).

98. Wang T, Wang G, Tan KE, Tan D. Spectral pyramid graph attention network for hyperspectral image classification. *arXiv preprint arXiv:200107108*, (2020).

99. Liu C, Cui J, Gan D, Yin G. Beyond COVID-19 Diagnosis: Prognosis with Hierarchical Graph Representation Learning. In: *International Conference on Medical Image Computing and Computer-Assisted Intervention*). Springer (2021).

100. De Matos J, Britto Jr AdS, Oliveira LE, Koerich AL. Histopathologic image processing: A review. *arXiv preprint arXiv:190407900*, (2019).

101. Gurcan MN, Boucheron LE, Can A, Madabhushi A, Rajpoot NM, Yener B. Histopathological image analysis: A review. *IEEE reviews in biomedical engineering* **2**, 147-171 (2009).

102. Zhou X, et al. A comprehensive review for breast histopathology image analysis using classical and deep neural networks. *IEEE Access* **8**, 90931-90956 (2020).

103. Zhou Y, Graham S, Alemi Koohbanani N, Shaban M, Heng P-A, Rajpoot N. Cgc-net: Cell graph convolutional network for grading of colorectal cancer histology images. In: *Proceedings of the IEEE/CVF International Conference on Computer Vision Workshops* (2019).

104. Anand D, Gadiya S, Sethi A. Histograms: graphs in histopathology. In: *Medical Imaging 2020: Digital Pathology*). International Society for Optics and Photonics (2020).

105. Keenan SJ, et al. An automated machine vision system for the histological grading of cervical intraepithelial neoplasia (CIN). *The Journal of pathology* **192**, 351-362 (2000).

106. Bilgin C, Demir C, Nagi C, Yener B. Cell-graph mining for breast tissue modeling and classification. In: *2007 29th Annual International Conference of the IEEE Engineering in Medicine and Biology Society*). IEEE (2007).

107. Sandler M, Howard A, Zhu M, Zhmoginov A, Chen L-C. Mobilenetv2: Inverted residuals and linear bottlenecks. In: *Proceedings of the IEEE conference on computer vision and pattern recognition* (2018).

108. Potjer FK. Region adjacency graphs and connected morphological operators. In: *Mathematical Morphology and Its Applications to Image and Signal Processing*). Springer (1996).

109. Xue Y, Xu T, Huang X. Adversarial learning with multi-scale loss for skin lesion segmentation. In: *2018 IEEE 15th International Symposium on Biomedical Imaging (ISBI 2018)*). IEEE (2018).

110. Wang G, Song T, Dong Q, Cui M, Huang N, Zhang S. Automatic ischemic stroke lesion segmentation from computed tomography perfusion images by image synthesis and attention-based deep neural networks. *Medical Image Analysis* **65**, 101787 (2020).

111. Qu H, et al. Weakly supervised deep nuclei segmentation using partial points annotation in histopathology images. *IEEE Transactions on Medical Imaging* **39**, 3655-3666 (2020).
112. Zhang J, et al. Joint fully convolutional and graph convolutional networks for weakly-supervised segmentation of pathology images. *Medical image analysis* **73**, 102183 (2021).
113. Zhao Y, et al. Predicting lymph node metastasis using histopathological images based on multiple instance learning with deep graph convolution. In: *Proceedings of the IEEE/CVF Conference on Computer Vision and Pattern Recognition* (2020).
114. Larsen ABL, Sønderby SK, Larochelle H, Winther O. Autoencoding beyond pixels using a learned similarity metric. In: *International conference on machine learning*). PMLR (2016).
115. Gao Z, Shi J, Wang J. GQ-GCN: Group Quadratic Graph Convolutional Network for Classification of Histopathological Images. In: *International Conference on Medical Image Computing and Computer-Assisted Intervention*). Springer (2021).
116. Levy J, Haudenschild C, Barwick C, Christensen B, Vaickus L. Topological feature extraction and visualization of whole slide images using graph neural networks. In: *BIOCOMPUTING 2021: Proceedings of the Pacific Symposium*). World Scientific (2020).
117. Jaume G, et al. Towards explainable graph representations in digital pathology. *arXiv preprint arXiv:200700311*, (2020).
118. Ying R, Bourgeois D, You J, Zitnik M, Leskovec J. Gnnexplainer: Generating explanations for graph neural networks. *Advances in neural information processing systems* **32**, 9240 (2019).
119. Sureka M, Patil A, Anand D, Sethi A. Visualization for histopathology images using graph convolutional neural networks. In: *2020 IEEE 20th International Conference on Bioinformatics and Bioengineering (BIBE)*). IEEE (2020).
120. Pati P, et al. Hact-net: A hierarchical cell-to-tissue graph neural network for histopathological image classification. In: *Uncertainty for Safe Utilization of Machine Learning in Medical Imaging, and Graphs in Biomedical Image Analysis*). Springer (2020).
121. Kumar N, Verma R, Sharma S, Bhargava S, Vahadane A, Sethi A. A dataset and a technique for generalized nuclear segmentation for computational pathology. *IEEE transactions on medical imaging* **36**, 1550-1560 (2017).
122. Graham S, et al. Hover-net: Simultaneous segmentation and classification of nuclei in multi-tissue histology images. *Medical Image Analysis* **58**, 101563 (2019).
123. Bodnar C, Cangea C, Lio P. Deep graph mapper: Seeing graphs through the neural lens. *arXiv preprint arXiv:200203864*, (2020).
124. Wojciechowska M, Malacrino S, Garcia Martin N, Fehri H, Rittscher J. Early Detection of Liver Fibrosis Using Graph Convolutional Networks. In: *International Conference on Medical Image Computing and Computer-Assisted Intervention*). Springer (2021).

125. Wang J, Chen RJ, Lu MY, Baras A, Mahmood F. Weakly supervised prostate tma classification via graph convolutional networks. In: *2020 IEEE 17th International Symposium on Biomedical Imaging (ISBI)*). IEEE (2020).

126. Wang Y, *et al.* Cell graph neural networks enable digital staging of tumour microenvironment and precisely predict patient survival in gastric cancer. *medRxiv*, (2021).

127. Li R, Yao J, Zhu X, Li Y, Huang J. Graph CNN for survival analysis on whole slide pathological images. In: *International Conference on Medical Image Computing and Computer-Assisted Intervention*). Springer (2018).

128. Chen RJ, *et al.* Whole Slide Images are 2D Point Clouds: Context-Aware Survival Prediction using Patch-based Graph Convolutional Networks. In: *International Conference on Medical Image Computing and Computer-Assisted Intervention*). Springer (2021).

129. Chen RJ, *et al.* Pathomic fusion: an integrated framework for fusing histopathology and genomic features for cancer diagnosis and prognosis. *IEEE Transactions on Medical Imaging*, (2020).

130. Wang Z, *et al.* Hierarchical Graph Pathomic Network for Progression Free Survival Prediction. In: *International Conference on Medical Image Computing and Computer-Assisted Intervention*). Springer (2021).

131. He K, Gkioxari G, Dollár P, Girshick R. Mask r-cnn. In: *Proceedings of the IEEE international conference on computer vision*) (2017).

132. Kather JN, *et al.* Deep learning can predict microsatellite instability directly from histology in gastrointestinal cancer. *Nature medicine* **25**, 1054-1056 (2019).

133. Kather JN, *et al.* Pan-cancer image-based detection of clinically actionable genetic alterations. *Nature cancer* **1**, 789-799 (2020).

134. Fu Y, *et al.* Pan-cancer computational histopathology reveals mutations, tumor composition and prognosis. *Nature Cancer* **1**, 800-810 (2020).

135. Lu W, Graham S, Bilal M, Rajpoot N, Minhas F. Capturing Cellular Topology in Multi-Gigapixel Pathology Images. In: *Proceedings of the IEEE/CVF Conference on Computer Vision and Pattern Recognition Workshops*) (2020).

136. Müllner D. Modern hierarchical, agglomerative clustering algorithms. *arXiv preprint arXiv:11092378*, (2011).

137. Shin SY, Lee S, Yun ID, Lee KM. Deep vessel segmentation by learning graphical connectivity. *Medical image analysis* **58**, 101556 (2019).

138. Noh KJ, Park SJ, Lee S. Combining fundus images and fluorescein angiography for artery/vein classification using the hierarchical vessel graph network. In: *International Conference on Medical Image Computing and Computer-Assisted Intervention*). Springer (2020).

139. Wu J, et al. Learning Differential Diagnosis of Skin Conditions with Co-occurrence Supervision Using Graph Convolutional Networks. In: *International Conference on Medical Image Computing and Computer-Assisted Intervention*). Springer (2020).
140. Meng Y, et al. CNN-GCN aggregation enabled boundary regression for biomedical image segmentation. In: *International Conference on Medical Image Computing and Computer-Assisted Intervention*). Springer (2020).
141. Islam M, Seenivasan L, Ming LC, Ren H. Learning and reasoning with the graph structure representation in robotic surgery. In: *International Conference on Medical Image Computing and Computer-Assisted Intervention*). Springer (2020).
142. Chen J, Yu B, Lei B, Feng R, Chen DZ, Wu J. Doctor Imitator: A Graph-based Bone Age Assessment Framework Using Hand Radiographs. In: *International Conference on Medical Image Computing and Computer-Assisted Intervention*). Springer (2020).
143. Li X, et al. Braingnn: Interpretable brain graph neural network for fmri analysis. *Medical Image Analysis* **74**, 102233 (2021).
144. Pope PE, Kolouri S, Rostami M, Martin CE, Hoffmann H. Explainability methods for graph convolutional neural networks. In: *Proceedings of the IEEE/CVF Conference on Computer Vision and Pattern Recognition*) (2019).
145. Hu W, et al. Strategies for pre-training graph neural networks. *arXiv preprint arXiv:190512265*, (2019).
146. You Y, Chen T, Sui Y, Chen T, Wang Z, Shen Y. Graph contrastive learning with augmentations. *Advances in Neural Information Processing Systems* **33**, 5812-5823 (2020).
147. Qiu J, et al. Gcc: Graph contrastive coding for graph neural network pre-training. In: *Proceedings of the 26th ACM SIGKDD International Conference on Knowledge Discovery & Data Mining*) (2020).
148. Dwivedi VP, Joshi CK, Laurent T, Bengio Y, Bresson X. Benchmarking graph neural networks. *arXiv preprint arXiv:200300982*, (2020).
149. Errica F, Podda M, Bacciu D, Micheli A. A fair comparison of graph neural networks for graph classification. *arXiv preprint arXiv:191209893*, (2019).
150. Hu W, et al. Open graph benchmark: Datasets for machine learning on graphs. *arXiv preprint arXiv:200500687*, (2020).
151. Zamanitajeddin N, Jahanifar M, Rajpoot N. Cells are actors: Social network analysis with classical ml for sota histology image classification. In: *International Conference on Medical Image Computing and Computer-Assisted Intervention*). Springer (2021).
152. Devlin J, Chang M-W, Lee K, Toutanova K. Bert: Pre-training of deep bidirectional transformers for language understanding. *arXiv preprint arXiv:181004805*, (2018).

153. Gao Y, Zhou M, Metaxas DN. UTNet: a hybrid transformer architecture for medical image segmentation. In: *International Conference on Medical Image Computing and Computer-Assisted Intervention*). Springer (2021).
154. Dosovitskiy A, *et al.* An image is worth 16x16 words: Transformers for image recognition at scale. *arXiv preprint arXiv:201011929*, (2020).
155. Bai R, *et al.* GCsT: Graph Convolutional Skeleton Transformer for Action Recognition. *arXiv preprint arXiv:210902860*, (2021).
156. Chaitanya K, Erdil E, Karani N, Konukoglu E. Contrastive learning of global and local features for medical image segmentation with limited annotations. *arXiv preprint arXiv:200610511*, (2020).
157. Xie Q, Luong M-T, Hovy E, Le QV. Self-training with noisy student improves imagenet classification. In: *Proceedings of the IEEE/CVF Conference on Computer Vision and Pattern Recognition*) (2020).
158. Liu X, *et al.* Generative self-training for cross-domain unsupervised tagged-to-cine mri synthesis. In: *International Conference on Medical Image Computing and Computer-Assisted Intervention*). Springer (2021).